R. & M. No. 3470

MINISTRY OF AVIATION

AERONAUTICAL RESEARCH COUNCIL
REPORTS AND MEMORANDA

Wind Tunnel Tests on a Streamlined Fan-Lift Nacelle

By J. E. HACKETT, Ph.D.

Part I.—Tests on Nacelle Alone and with Wings or Underfins Fitted

Part II.—The effect of Forward Speed on the Lift Produced by a Lifting Fan and its Inlet

LONDON: HER MAJESTY'S STATIONERY OFFICE
1967

PRICE £1 0*s.* 0*d.* NET

Wind Tunnel Tests on a Streamlined Fan-Lift Nacelle

By J. E. HACKETT, Ph.D.

Part I.—Tests on Nacelle Alone and with Wings or Underfins Fitted

Part II.—The effect of Forward Speed on the Lift Produced by a Lifting Fan and its Inlet

Reports and Memoranda No. 3470*
October, 1965

Summary.

Part I describes tests on a streamlined body with a lifting fan mounted normally to its axis. Most of the tests were made in the 5 ft × 4 ft wind tunnel at Imperial College, and others in the No. 1 $11\frac{1}{2}$ ft × $8\frac{1}{2}$ ft. tunnel at R.A.E. Farnborough. Comments are made on model design and engineering.

Three component balance measurements and flow visualization were carried out over a range of ± 20 deg. incidence at speeds from 15 to 65 per cent of the jet velocity, keeping fan r.p.m. constant. Comparison between tunnels showed important differences at high incidences and high forward speeds (18 deg. and $V/V_J = 0{\cdot}6$) but 2 to 3 per cent or less at lower speeds and incidences.

Part II analyses in more general terms the way in which forward speed changes affect the lifting unit and the forces on it and examines the properties of hypothetical lifting units which have constant pressure and constant volume characteristics. The former is found to have some desirable features.

The analysis is then applied to the experimental results from Part I, showing that, at a typical transition speed, a 5 per cent lift loss due to fan-mainstream interaction is less significant than, say, the addition of underfins which influence the efflux-mainstream interaction.

LIST OF CONTENTS

Section

1. Introduction to Parts I and II

PART I

2. The Model and its Design
   - 2.1 Model shape
   - 2.2 Model size and jet velocity
   - 2.3 Mechanical design
   - 2.4 Vibrations and resonances
3. Experimental Scope and Procedure
4. Datum Tests, Fan Off and Static Lift

*Replaces N.P.L. Aero Reports 1152 and 1170—A.R.C. 26,969 and 27,330.

LIST OF CONTENTS—*continued*

5. Flow Observations and Duct Flow Measurements with Fan On
   5.1 Interaction between the jet and the 5 ft × 4 ft wind tunnel
   5.2 The jet plume
   5.3 Surface flows
   5.4 Flow through the duct
6. The Results of Force Measurements, Fan On
   6.1 Plain body
   6.2 Body with wings
   6.3 Drag and pitching moment
7. Wind-Tunnel Interference
   7.1 Plain body
   7.2 Body with wings
   7.3 Drag and pitching moment increments

PART II

8. Theoretical Forces on a Fan and Shroud at Forward Speeds
   8.1 Fan lift
   8.2 Theoretical shroud force at zero forward speed
   8.3 Shroud lift at forward speed
   8.4 Drag and pitching moment at forward speed
   8.5 Extension to multiple intakes
9. Application to Fan Systems
10. Fan interaction and Total Lift Loss for the Streamlined Nacelle Wind Tunnel Model
11. Conclusions
   11.1 Conclusions to Part I
   11.2 Conclusions to Part II
12. Acknowledgements
13. Notation

References

Tables 1–3

Illustrations Figs. 1–37

Detachable Abstract Cards

1. *Introduction to Parts I and II.*

This report combines References 19 and 20 as Parts I and II respectively.

Part I will describe experiments on a streamlined nacelle with a lifting fan fitted at a distance 40 per cent of the nacelle length back from the nose. In Part II a broader analysis will be applied to determine the effect of forward speed on the lifting unit. The results from Part I will be quoted in Part II by way of example.

The work was originally carried out in 1961 and 1962 (*see* Table 2) at a time when there was considerable emphasis on suction effects which exist to the rear of lifting jets emerging from a flat surface into a cross flow[7,8,9,10] – such as a lifting fan in a wing. Because of this, emphasis tended towards body-mounted lifting units[5,10,11]. The work described in Part I was carried out in parallel with the latter experiments, the object being to reduce further the horizontal area around the jet, in the hope that adverse interference would also be reduced. A clearer understanding of the aerodynamics was also sought.

Part II highlights a further, but usually less significant, cause of lift loss at forward speed for, as forward speed increases, it will be seen that the increased inlet total head and the changed outlet conditions result in a decreased total head rise across the fan and an attendant increase in the flow through the fan at constant r.p.m., consistent with its total-head rise characteristic. The resultant changes in lift and drag on the fan unit (including the intake) will be examined.

Part I.—Tests on Nacelle Alone and with Wings or Underfins Fitted

2. *The Model and its Design.*

2.1. *Model Shape* (*see* Figs. 1 and 2).

In an attempt to achieve a low drag coefficient with fan off, the shape of the body was derived from the airship R.101, the fan axis being at right angles to the body centreline. In order to reduce lateral velocity components, which might have affected the fan, (and which would have complicated traverses across the duct for the determination of mass flow) the sides of the body were built up to form 'high-light' areas in end planes normal to the duct axis. It was thus possible to make the body diameter only about 30 per cent greater than that of the duct and to leave only a small horizontal area around the outlet of the duct (*see* Figs. 1 and 2). In order to promote attached flow over the intake lip this was given a generous radius (one fifth of fan diameter) on the upstream side of the inlet, reducing to 6 per cent at the sides and rear of the duct. Table 1 gives a summary of model dimensions.

Because of mechanical problems associated with the high rotational speeds which were found to be necessary, a single-fan lifting unit was used with straighteners after the fan. This was placed one quarter of a diameter from the inlet plane so that any separations from the intake lip at high forward speeds should not have become too large before the fan was encountered. Mechanical considerations also showed that this position was preferable and in addition it may be reasonably representative of full-scale practice. The centrebody, 58 per cent of the duct diameter, was a short cylinder with ellipsoidal ends.

Wings could be added of such a size that transition from jet- to wing-supported flight would be possible when the forward speed was one third of the jet speed. The aspect ratio of 6 and taper ratio of 0·5 gave an approximately elliptical spanwise lift distribution with the model fan switched off and the duct ends sealed. Provision was made for the wing-body angle to be varied within the range ± 30 deg.

The detachable underfins shown in Fig. 1 were flat plates made of Perspex, sealed along their upper edges against the body.

2.2. *Model Size and Jet Velocity.*

The way in which aerodynamic and experimental factors affected model size and jet velocity is summarised by Fig. 3. The range of possible designs was severely restricted by considerations of jet velocity ratio, fan tip Mach number and the size of the motor, which had to be housed in the forebody. In plotting the line AB allowances have been made for mechanical and fan efficiencies and a 58 per cent fan boss has been assumed.

Although the dictates of motor size caused the model to become somewhat larger than was desirable in the 5 ft × 4 ft tunnel, the ratio of jet diameter to tunnel height was about the same as for most similar experiments then being performed elsewhere. The above considerations indicated that no model fan unit then existing would have been small enough so a new design was undertaken.

The fan was designed by the free-vortex method and by keeping blade angles moderate it was hoped to reduce adverse effects due to inlet maldistribution and cross flow. Both the fan boss diameter and the rotational speed were strongly influenced by the consequent decision to limit the local advance ratio at the boss to about 0·60.

The design r.p.m. and jet velocity were so chosen that standard frequency-changing equipment could be used to give a constant 400 c/s supply and 24 000 synchronous r.p.m. The fan tip diameter was chosen so that a slightly larger motor could be installed than was strictly necessary.

2.3. *Mechanical Design*

The aim throughout the design was to avoid development problems, so a conservative approach was adopted using standard parts and techniques as much as possible. However, the engineering problems of the high rotational speed had to be faced.

After considering several non-electrical alternatives a standard three-phase squirrel-cage Stator-Rotor unit was chosen of a type normally built into machine tools, since space could then be saved by building the motor as an integral part of the model. The unit was also sufficiently cheap to be regarded as expendable so that it could have been overloaded if necessary to give substantially more power at reduced life. However, the unit was run within the 'ventilated' rating of 6 h.p. and was cooled by air drawn in through the nose of the model. The motor stator length and diameter were 9·0 in. and 4·5 in., the largest length to diameter ratio available.

The motor housing and fan duct section were machined from aluminium alloy castings giving good rigidity and making easier the alignment and the achievement of the close tolerances required for high-speed running. The fan was made from an aluminium alloy casting, the blades being profiled on a copying and reducing machine.

The right-angled spiral-bevel gears needed to transmit 6 h.p. at 24 000 r.p.m. so nearly filled the space available in the centrebody that only a 1 : 1 ratio could be chosen. However, their bulk was justified by their trouble-free performance.

2.4. *Vibrations and Resonances*

High imposed frequencies made necessary a careful survey of the natural frequencies of the major moving parts and design philosophy was to keep the fundamental frequencies below those imposed whenever possible. However, the fan blade bending mode required considerable care because of imposed frequencies which straddled both the fundamental and the third harmonic. The blade was tapered slightly in thickness and planform both to alleviate a fatigue problem and to raise the fundamental bending frequency. The problems were slightly eased because input frequency was not variable and start up and shut down were very rapid (about a second). Shaft whirling speeds were also checked and the combination of a long motor with a cantilevered drive made relatively large shaft diameters necessary to raise the whirl speed above the running speed. This accounts for the unwelcome presence in the fan duct of a thick shaft which, because of its 88 ft/sec surface speed, and relatively large diameter, had to be shrouded to avoid Magnus effect.

3. *Experimental Scope and Procedure.*

Table 2 summarises tests performed at Imperial College and at R.A.E. Farnborough during 1961 and 1962. The former were made at a series of constant incidences, which avoided changes of balance zero during a run, but at Farnborough the tunnel speed took too long to settle for this to be convenient. Tests there were not possible at about 100 ft/sec because of a tunnel resonance. The model fan ran at approximately 23 000 r.p.m. in all tests, measured as fan blade noise frequency, which could be determined accurately.

Crossed bracing wires had to be added to the standard tunnel struts originally used (Fig. 2), in order to suppress sideways oscillations with fan and tunnel running. No strut guards were used and strut drags of 40 per cent of total drag were measured at 100 ft/sec with the fan on. Strut drag was measured with a cylinder spanning the struts to represent the mounting spindles of the configuration without wings, an appropriate correction being made for the portion spanning the body position. The cylinder was removed for determination of the strut drags for the winged configuration. The tail wires supplied three phase power to the fan motor.

Tunnel speed was determined from the pressure drop across the contraction. A vertical rake of pitot and static tubes showed no change of centreline distributions upstream of the model when the model fan was run and little change of calibration factor. Fortunately any changes in calibration factor occurred where fan-off force coefficients were small and no corrections were needed.

Pitot and static rakes were so arranged halfway down the duct as to give the coverage shown in Fig. 4, spacing being on an equal area basis. They were inclined into the fan mean swirl at 15 deg to the axial direction, giving calculated misalignment of ± 3 deg for the end tubes at zero forward speed. The effect of changes of forward speed and incidence on flow direction is not known in detail but measurements by Gregory[6] indicate that errors of significant size are probably confined to small areas.

The pressure tubes were connected to a vertical multitube manometer, containing carbon tetrachloride, which had scales with alternate black and white markings which enabled photographs of the manometer on film to be processed automatically by a specially designed reader[3]. No individual tube calibrations were applied since these were within 1 per cent of each other, which is comparable with probable errors due to flow misalignment.

4. *Datum Tests, Fan Off and Static Lift*

Figs. 5, 6 and 7 show the lift, drag and pitching moment characteristics with fan off for all configurations, measured in the R.A.E. No. 1 $11\frac{1}{2}$ ft $\times$ $8\frac{1}{2}$ ft wind tunnel unless otherwise stated.

Because the model was a thickened version of the R.101 with the maximum thickness further back (at 40 per cent length), comparisons between R.101 model tests and the present plain body measurements (i.e., without wings or underfins) were unlikely to be fruitful. However, calculations using Ref. 13 to predict lift were within 10 per cent of experimental measurements provided allowance was made for the variation of cross-flow Reynolds number with incidence. (Half the maximum diameter was used as the length scale).

Favourable interference almost doubled body lift at a given incidence when underfins were fitted but there was a large increase in drag. The addition of wings gave an overall lift-curve slope between 5 and 10 per cent below that calculated[14] for the equivalent wing extending across the body, but prediction is difficult at the mean chord Reynolds numbers around $0{\cdot}4 \times 10^6$.

The zero-lift drag coefficient of the isolated body was consistent with the data given by Goldstein[15] but a decrease with incidence as quoted by Thwaites[13] for a model of the airship 'Akron' did not occur. Natural transition occurred on the present model just ahead of the raised shoulders around the duct. The lift-dependent drag of the wing and body combination was about double that predicted for the wing alone, resulting in a maximum lift : drag ratio of approximately 7·5.

The plain body pitching moments were about 30 per cent higher than quoted for the 'Akron' model[13] at the same lift coefficient. The addition of wings, with their quarter chord at the model pivot, caused little change until the stall.

4.1. *Static Lift*

Fig. 8 gives a breakdown of lift losses, both within the duct and externally due to fitting wings, etc., and due to making measurements in a closed tunnel. The lift on the plain body is taken as standard.

Early static lift readings for the plain body were more than 1 lb lower than the design value, even though all the doors and windows of the tunnel had been opened. (The tunnel floor was 3·2 diameters below the jet exit.) Inclining the model to ± 20 deg incidence did little to reduce the recirculation and ground effect which probably caused the deficit. An 18 in. diameter hole was therefore cut in the tunnel floor to allow the jet to escape. The static lift on the plain body was then close to the predicted value.

Fig. 8 shows that, according to balance measurements, the presence of wings reduced the static lift by about $1\frac{1}{2}$ per cent, probably due to ground effect. The addition of underfins caused a further reduction of about 3 per cent.

The static lift coefficients in the 5 ft × 4 ft tunnel when (a) fully closed and (b) with vented floor and walls, were respectively $\frac{T}{\rho(\Omega R)^2 A_J} = 0{\cdot}0850$ and 0·091. The corresponding values in the $11\frac{1}{2}$ ft × $8\frac{1}{2}$ ft tunnel were 0·0845 and 0·090.

Bearing in mind the greater distance to the floor and the longer recirculation path, one would expect the thrust coefficient in the closed working section of the larger tunnel to be close to the vented value in either tunnel. While the observed agreement between the vented tunnel results is to be expected, it is difficult to explain the change due to closing the larger tunnel. Possibly the complete absence of wall venting was in some way responsible.

It is clear that when measuring static lift great care is necessary to vent the working section adequately. Because of the above unexplained features, fan tip-speed parameters have been used to reduce force increments for comparisons between the two tunnels in Section 7.

5. *Flow Observations and Duct Flow Measurements with Fan On.*

5.1 *Interaction Between the Jet and the 5 ft × 4 ft Wind Tunnel*

Upstream static-pressure measurements and floor wool-tuft observations were made over the range of test parameters. These gave indications of conditions under which the flow near the model might be noticeably different from that in free air. At low forward speeds stagnation occurred when the jet hit the tunnel floor and a region of separated flow there increased in extent as the model incidence was raised. This accompanied a rise in static pressure at the standard tunnel static holes at the beginning of the working section. The effect was superimposed on an existing pressure gradient present due to lack of area compensation for tunnel boundary layers. Except in the floor stagnation cases the size of this gradient was reduced by fan operation. As the pressure rise was only a few millimetres of water the resulting horizontal buoyancy forces on the model were small. However, Fig. 9 shows that the static-pressure rise due to fan operation was a large proportion of tunnel dynamic pressure and was strongly related to the extent of separation on the tunnel floor.

As forward speed increased floor stagnation disappeared but the static-pressure rise ahead of the model continued to increase. However, the forces on the model due to changes in pressure gradient were still less than 1 per cent of fan static lift. It is apparent that local effects caused by floor stagnation at low forward speeds are more significant than the longitudinal pressure gradient. A rise in static pressure below the forebody may be expected to increase all the measured increments at positive incidences. The extent of the floor separation (Fig. 9) corresponds closely to differences between increments measured in the 5 ft × 4 ft and $11\frac{1}{2}$ ft × $8\frac{1}{2}$ ft tunnels.

The solid blockage effect of the model alone gave calculated local velocity increases of about $\frac{1}{2}$ per cent which rose to almost 1 per cent when a jet cylinder extending to the floor was assumed. Because the volume and shape of the jet plume were variable and unknown in general, no attempt could be made to estimate wake blockage.

5.2. *The Jet Plume*

Jordinson[17] shows that as a round jet emerges normally from a flat plate into a stream it is bent over, its cross section being distorted into a kidney shape and then into a horseshoe shape. The results of tests using a tuft grid and with smoke are summarized by Figs. 10 and 11. The edge of the region of disturbed flow in Fig. 10 is clear of the floor only in the high forward speed case. It appears likely that the penetration and the shape of the plume in the other cases are affected by floor constraint. Unfortunately no similar observations were made in the R.A.E. $11\frac{1}{2}$ ft. × $8\frac{1}{2}$ ft tunnel to confirm this.

A possible plume structure, deduced from the limited flow observations above, will now be described. The edges of a viscous jet directed downwards in still air may be represented by a series of coaxial vortex rings. As the speed of a horizontal mainstream is increased the downstream sides of the vortex rings

are carried away, leaving a trailing vortex system. The process is analogous to vortex shedding by an accelerating wing. Fig. 11 shows the resulting flow structure in which the vortex sheet towards the back of the jet rolls up as it is stretched and convected downstream to form the vortex pair of Fig. 10.

5.3. *Surface flows.*

In addition to the downwash field over the rear of the body, associated with the trailing vortices in the jet plume, local effects existed near the jet which combined the flow around the jet cylinder with suctions due to mixing. The flow characteristics around the front of the jet were similar to those to be expected on the equivalent cylinder-body junction. However, the flow to the rear was strongly affected by jet suction since it was shielded from the mainstream. This was particularly marked with underfins added which delayed closure of the mainstream behind the jet.

The flow patterns produced at zero incidence showed a general resemblance to the corresponding patterns around a jet issuing normally from a flat plate[18]. Comparison between Figs. 12 and 13, for medium and high forward speeds, shows that the local influence of jet suction was only slightly less marked at the higher mainstream speed. In regions of the afterbody less subject to local jet-suction effects the surface flow angles varied little with forward speed. Since clearance between the jet and the body decreased with forward speed it may therefore be inferred that there was a simultaneous reduction in the strengths of the vortices. It could be seen from tuft photographs that the vortex helix angles decreased as forward speed increased.

The flow patterns were generally more affected by changes in incidence than changes in speed. At negative incidences flow patterns became more complicated with as many as five singular points present on the surface around the jet in some cases[3]. At high positive incidences there appeared to be vortex rooting behind the jet at all the forward speeds at which patterns could be produced. However, force measurements showed that tunnel constraint forces accompanied the apparent vortex rooting but unfortunately no visualization was carried out in the $11\frac{1}{2}$ ft $\times$ $8\frac{1}{2}$ ft tunnel to ascertain whether or not this was solely a tunnel effect.

At zero incidence patterns with and without wings were very similar. At positive incidences flow behind the jet closed more readily, probably due to positive pressures below the wing. Simple flow patterns resulted right up to $+20$ deg incidence. The reversed flow region above the wing of Fig. 12e resembled that with the fan off.

When the wing stalled negatively parts of the body in its wake became strongly affected by jet suction. Fig. 12a shows that there was extensive reversed flow behind the jet at -20 deg incidence.

It was found that with the fan off and the duct sealed at zero incidence the flow over the underfins was uniform on both sides with no bubbles or edge separations. With the fan on, surface flow patterns showed that the sides of the jet became attached to the inside of the fins. This caused mainstream air to be deflected downwards between the fins (*see* Fig. 14b), leaving a region of slow-moving air on the undersurface of the body just ahead of the jet.

Fig. 14c was obtained by allowing the pigment in paraffin applied to the outside of the fins to be carried to the cleaned inner surface. The outside pattern was then rubbed off to show the reversed flow region on the fins behind the jet. There was also a corresponding reversed flow region on the body.

Patterns produced by an edge vortex outside the lower edge of the fin can be seen in Fig. 14a; these were not visible at zero and negative incidences. Although no evidence is available to support the view, it seems likely that this became an alternative starting point for the vortex system found earlier. If this was so the displacement of the trailing vortices away from body surfaces could have reduced adverse downwash effects.

5.4. *Flow Through the Duct.*

The inlet flare consisted of a 20 per cent radius on the upstream side of the duct, which decreased steadily to 6 per cent of jet diameter at the sides and rear of the duct as shown in Fig. 15. Also shown in this figure are areas where, at the central plane beneath the fan, manometer readings fluctuated. In general the amplitude of these fluctuations was much smaller than the mean reading of total head, which was a little lower than nearby tubes.

A further indication of the performance of the inlet flare at forward speed was given by Dayglo and paraffin flow visualization. Because of gravity and three-dimensional effects the interpretation of these patterns was difficult and photography was impossible. However, there was a correspondence between the small areas of apparent separation below the inlet flare and the regions where the manometer readings fluctuated. Taking both sets of observations together it seems reasonable to infer that the lip radii should have been larger in the regions around 45 deg each side of the forward centreline. However, less than 2 per cent of the area behind the fan was affected.

With the single exception of the exit traverse at zero forward speed (Fig. 17) all flow measurements were at the central plane which contained the drive shaft. The traverse plane was chosen so as to avoid errors in total-head-rise coefficients which would have resulted from putting the probes too close to the fan (*see* Ref. 16). It was also desirable to place the probes upstream of the straighteners to prevent confusion with wakes. Fig. 18 shows that, under static-lift conditions, the observed total-head-rise coefficients agree fairly well with those predicted for the measured flow coefficients. The drop in total head beneath the blade tip is thought to have been due to an accumulation of blade and duct boundary-layer air, rather than tip loss, since tip clearance was small. A tip Mach number of 0·6 should have given no drag-rise penalty and a lift coefficient expected to be less than 0·6 should not have caused stalling.

The uniformity of the flow in the central plane was good away from the drive shaft, which also created a large wake at the exit plane. The rotation and twisting of this wake between the central plane and the straighteners was close to that predicted using design figures.

At the exit plane static pressure decreased from atmospheric at the edge of the jet to about 1 in. water suction near the centrebody ($C_p \simeq -0{\cdot}10$). No residual swirl could be seen using a tuft grid though, on the basis of calculations made after completion of testing, up to 5 deg underturning might be expected.

The static pressure indicated by both the wall holes and the static probes at the central plane was approximately atmospheric, showing that the diffuser and straightener pressure rises were nullified by losses.

Finally, Fig. 19 shows the effect of forward speed on fan performance, including power input. The fan progresses down its total-head-rise characteristic curve as forward speed increases, with decreases in total-head rise and power input while mean velocities increase. The attendant changes in incremental lift and drag are fully discussed in Part II, and will be referred to in the following Section.

6. *The Results of Force Measurements, Fan On* (*see* Figs. 20 to 28 and Table 3)

6.1. *Plain Body*

There are several important mechanisms which affect the incremental lift on the model. These include variation of fan blade incidence as external conditions change and flow distortions due to the emergent jet.

The significant property of an axial-flow fan is that a small increase in axial speed produces quite a large change in blade lift and pressure rise, giving the familiar steep total-head-rise curve. Consider the effect of increasing the speed of the mainstream while holding fan r.p.m. constant. It has been found experimentally (Ref. 3) that upstream rather than downstream effects dominate the fan aerodynamics in this situation. Since the total head of the flow approaching the fan is increased and since changes in axial velocity are small (zero for a vertical characteristic), it follows that the static pressure ahead of the fan must rise by an amount slightly less than the mainstream dynamic head. Ref. 4 illustrates this effect in more detail but the upper graph in Fig. 19 shows how the total-head rise, and hence the lift on the fan, decreases as forward speed increases. For the present fan an increase of lift on the intake due to the small increase in axial velocity is smaller than the sum of loss of fan lift and the increase in the drag of obstructions in the duct. There therefore results a decrease in the lift increment on the fan unit as forward speed increases.

A second effect concerns the interaction of the jet with the mainstream which produces suctions around the exit and cross-flow over the rear body. In Ref. 3 a crude vortex model of the jet plume is presented which relies on information from surface-flow photographs of the circular rear fuselage. It is shown there that cross-flows over the body due to the jet plume are of the right magnitude to account for the remainder of the initial lift loss with forward speed.

The increase in incremental lift which starts at a forward speed of about one third of the jet speed, shown in Figs. 20 and 26, is not explained by either of the above mechanisms. It is certainly not due to the fan interaction of the sort described in Part II, but the possibility cannot be excluded at this stage that the crude jet-plume model of Ref. 3 is inadequate at the higher forward speeds. However, it is more likely that an induced-circulation effect is responsible. It seems fairly clear that some of the forces due to the addition of underfins (Figs. 22 and 23) are achieved in this way and it is possible that a similar but smaller effect may occur in their absence. The underfins also probably reduce the entrainment near the body and, by moving the trailing vortices away from the rear body, reduce the downwash over it. As mentioned in Part II it seems that from an aircraft performance point of view the use of underfins to produce lift benefits has more significance than any measures to alleviate loss of lift on the fan at forward speed.

6.2. *Body with Wings* (Fig. 21).

While lift increments both with and without wings vary more with incidence than with forward speed (*see* Fig. 28), the change due to the addition of wings to the isolated body depends mainly upon forward speed (*see* Fig. 27).

For all incidences at low forward speeds and at + 18 deg incidence at all the speeds of the tests, the addition of wings changed lift increment very little. As forward speed increased the 'lift bucket' at moderate incidences occurred earlier with wings fitted than without. Although the 'bucket' was up to 8 per cent deeper there was a more rapid recovery of lift after it. At − 18 deg incidence the operation of the fan delayed the negative wing stall and lift increments fell sharply. However, total lift variation was less violent.

During the first test series, forces were measured over a range of wing-setting angles in order to determine the effect of wing incidence independently of body angle. Fig. 27 is arranged so that equal wing incidences are on a vertical line. The dependence of lift increment on wing incidence is plainly demonstrated near the stall, but any possible interpretation in terms of flow fields is complicated by constraint effect in the 5 ft × 4 ft tunnel.

The observed decrease in spanwise spacing between the trailing vortices as forward speed increased (Fig. 10) should decrease the area of wing affected by downwash between the vortices and increase the area with upwash outside the vortex centres. One can imagine there being a forward speed at which the positive lift induced near the tips is equal to the downward force induced nearer the root. Below this forward speed the addition of wings to the plain body would reduce incremental lift while above it there would be an increase. This is consistent with the upper half of Fig. 27. The more local influences of jet entrainment and flows induced near the intake must also contribute to some extent, but with the present mid-wing the effects may not be large.

6.3. *Drag and Pitching Moment* (Figs. 24 and 25)

With the exception of domains in which tunnel constraint or stall effects were present the drag increments for all configurations were equal, to within the limits of measurement. This is somewhat surprising for the case with underfins in view of increased pressures ahead of the jet, but it appears that this is offset by a less rapid rise in momentum drag associated with the slower increase of jet velocity with forward speed with underfins fitted (Fig. 19).

Pitching-moment increments share several properties with those of drag though incidence dependence is less straightforward. Since moment increments are in part associated with the removal of mainstream momentum from above the intake, an approximately linear variation with forward speed can be expected. In practice (Fig. 25) the lines are slightly curved, probably in association with incremental lift variations.

7. *Wind-Tunnel Interference* (Figs. 20 to 25 and Table 3)

7.1. *Plain Body*

It can be seen from Fig. 26 that the loss of lift with forward speed rarely exceeds 10 per cent of the static lift and a comparison of full and broken curves shows that a noticeable proportion of this is due to loss of lift on the fan-shroud combination. This illustrates that paring away the area around the jet exit was quite successful in reducing lift loss due to entrainment and due to downwash between the vortices in

the jet plume. It also follows that the image vortices, reflected in the floor, will produce interference forces which are even smaller. In fact a calculation within the same crude framework as that of Ref. 3 showed that velocities induced by the image vortices were only one or two per cent of those induced by the real vortices, which themselves induced forces only of order 5 per cent of total lift.

Although the above approach probably indicates correctly the order of magnitude of interferences due to the trailing vortices, further qualifications are needed.

Firstly, because the jet-plume system is not yet sufficiently understood, no attempt was made to ensure that the real and image vortex systems were in equilibrium, and the penetration of the jet plume into the stream may have been affected by the tunnel floor to a greater extent than indicated by the image vortex system used above. There is a temptation to compare the present work with that of Jordinson[17] but there are several difficulties. The scale of his experiments was much smaller and his jet was 'solid' and directed from a wall, while the present jet was directed from a slender body and its core contained the wake of the centrebody. Jordinson gives the penetration of a line of maximum total head, whereas only vortex-centre positions are available here. Nevertheless, it is found that the penetration of the present vortex centres in terms of ' equivalent solid jet diameters' is about 65 per cent of the penetration of Jordinson's mean total-head line. Since the vortices are known to lie nearer to the jet outlet than the maximum total-head line does, the inference may be drawn that the penetration of the present jet in the small tunnel at V/V_J of 0·27 and above was at least 65 per cent of the free-air value even though the exit was only 3·2 diameters from the floor.

The second qualification is that the general nature of the flow should not be affected by the tunnel, in particular the jet should not form a stagnation point on the floor. Fig. 9 shows that with combined low speed and high incidence the jet did in fact hit the floor. It was seen in Section 4 that a loss in static lift of about 7 per cent occurred with the tunnel closed. At one fifth of jet speed, the lowest in the 5 ft × 4 ft tunnel, this had decreased to 2 or 3 per cent for the isolated body (Fig. 20). However, at this forward speed the situation was becoming more complicated, particularly with wings or underfins fitted.

7.2. *Body with Wings*

As was mentioned in the discussion of the winged configuration in Section 6, a proportion of each lift increment is associated with changes in wing incidence induced by the jet. Tunnel constraint in the 5 ft × 4 ft tunnel with fan off is sufficient to make conventional corrections desirable. Therefore, with the fan on, the tunnel constraint may influence the amount of induced incidence to a greater extent. This may happen in a manner which cannot be predicted using standard tunnel-correction techniques. As with the body without wings, constraint which changes with jet inclination may also be encountered at high incidences.

A further effect which may influence the comparison is the variation of wing stalling angle with tunnel constraint, forward speed and turbulence level. Any of these may influence the extent of separation induced on the wing by a particular jet configuration. In incremental plots this might appear as differences between tunnels in the conditions needed to produce rapid changes in lift increment, due to the stall.

In view of these considerations worse agreement is to be expected between tunnels than for the body without wings and Fig. 21 shows this to be so. Agreement is good only at low speeds and at low incidences. At most incidences lift recovery with forward speed starts sooner giving up to 15 per cent more lift increment in the smaller tunnel. Agreement was within ± 3 per cent at moderate incidences for $V/\Omega R$ up to 0·10.

7.3. *Drag and Pitching Moment Increments*

Agreement between drag increments was good up to + 6 deg incidence where the increments in the smaller tunnel started to rise from the linear characteristic obtained in the $11\frac{1}{2}$ ft × $8\frac{1}{2}$ ft tunnel. It is thought that floor stagnation is chiefly responsible at low speeds and that deviations at higher speeds at high incidence are associated with the lift discrepancies mentioned above.

There was considerable scatter in pitching-moment increments in both tunnels. However, the increments measured at R.A.E. were generally lower and varied less with incidence. The incidence effects occurred under the same conditions as did the lift and drag discrepancies, but the reason for a slight overall shift is not apparent.

Part II.—The effect of Forward Speed on the Lift Produced by a Lifting Fan and its Inlet

8. *Theoretical Forces on Fan and Shroud at Forward Speeds*

8.1. *Fan Lift.*

The analysis which follows is idealised in several aspects. The effects of inlet maldistribution and cross-flow at the fan have been ignored. Inlet losses have also been neglected. It is demonstrated in Ref. 4, for example, that this is reasonable for intakes without guide vanes provided that separations from the upstream lip do not occur at forward speed.

The force on the lifting unit is divided between the fan itself and the shroud. The force on the fan-straightener combination is readily obtained as

$$L = A_J \Delta H. \tag{1}$$

The calculation of the lift force on the shroud is less straightforward. It will be seen in the analysis which follows that momentum arguments valid at zero forward speed may not be used with a free stream present, though the same result would be obtained. In the present analysis it is necessary to assume that, in the separate zero forward speed and zero inlet flow cases, there is fore and aft symmetry about a transverse plane through the duct axis. It will also be assumed that these flow fields may be superposed.

8.2. *Theoretical Shroud Force at Zero Forward Speed*

Consider a flow field which is symmetrical about the duct axis as for the three-dimensional circular intake shown in Fig. 29.

Area of spherical surface AED $= 2\pi r^2(1-\cos\Theta)$,

therefore $$v = \frac{A_J V_J}{2\pi r^2(1-\cos\Theta)}, \text{ by continuity.}$$

Downward Vertical Momentum flux through an elementary ring of fluid

$$= (2\pi r \,.\, r d\theta \,.\, \rho v) \,.\, v \sin\theta$$

Total downward Vertical Momentum flux entering through AED

$$= \operatorname*{Lim}_{r\to\infty} \int_0^{\Theta} 2\pi r^2 \rho v^2 \sin\theta \, d\theta$$

$$= \operatorname*{Lim}_{r\to\infty} \frac{2\pi r^2 \rho (A_J V_J)^2}{4\pi^2 r^4 (1-\cos\Theta)^2} [\cos\theta]_0^{\Theta}$$

$$= \operatorname*{Lim}_{r\to\infty} \frac{\rho (A_J V_J)^2}{2\pi r^2 (1-\cos\Theta)}$$

$$= 0. \tag{2}$$

Notice that the above result is independent of Θ and is thus true for an intake in a flat surface and for a shroud ring, provided that this has sufficient frontal area to sustain the lift given by (3) below. Θ may also vary around the duct periphery so that the analysis holds equally for a flush intake into a fuselage or nacelle. However, slight error will result from the finite extent of practical shapes.

Consider the downward flux of vertical momentum through the control volume *ABCDE*, taking as a datum $p = 0$ at infinity and noting that $p_J = -\frac{1}{2}\rho V_J^2$ on this basis.

$$\oint (p+\rho V^2) = 0, \quad \text{i.e.}$$

$$\int_0^{\Theta} 2\pi r^2 \rho v^2 \sin\theta d\theta - \int_{A,C}^{B,D} p\,ds \quad - \int_B^C (p_J - \rho V_J^2)\, dA_J = 0$$

(DEA) (Force on air due to shroud) (BC)

i.e. 0 [from (2)] $- \int_{A,C}^{B,D} p\,ds - \frac{1}{2}\rho V_J^2 A_J = 0$

i.e. Shroud lift $L_S = \frac{1}{2}\rho V_J^2 A_J$ (3)

8.3. *Shroud Lift at Forward Speed V*

Consider a point A on a three-dimensional shroud (Fig. 30) where the components of the surface flow velocity are u, v and w in the x, y and z directions respectively.

Define

q_V as the local surface velocity with the free stream acting alone

q_J as the local surface velocity with the intake working in the absence of a free stream

q_{VJ} as the local surface velocity with the intake working in the presence of a free stream

then $q_V^2 = u_V^2 + v_V^2 + w_V^2$

$q_J^2 = u_J^2 + v_J^2 + w_J^2$

$q_{VJ}^2 = u_{VJ}^2 + v_{VJ}^2 + w_{VJ}^2 = (u_V+u_J)^2 + (v_V+v_J)^2 + (w_V+w_J)^2$

if the flow fields may be superposed,

i.e. at point A

$$q_{VJ_A}^2 = q_{J_A}^2 + q_{V_A}^2 + 2u_{V_A}u_{J_A} + 2v_{V_A}v_{J_A} + 2w_{V_A}w_{J_A}.$$

Now, using Bernoulli's equation, and measuring pressures above the value at infinity,

$p_{A_V} = \frac{1}{2}\rho V^2 - \frac{1}{2}\rho q_{V_A}^2$ due to the free stream acting alone

$p_{A_J} = -\frac{1}{2}\rho q_{J_A}^2$ due to the intake alone

$p_{A_{JV}} = \frac{1}{2}\rho V^2 - \frac{1}{2}\rho q_{VJ_A}^2$ due to both acting together

$= \frac{1}{2}\rho V^2 - \frac{1}{2}\rho q_{J_A}^2 - \frac{1}{2}\rho q_{V_A}^2 - \rho u_{V_A}u_{J_A} - \rho v_{V_A}v_{J_A} - \rho w_{V_A}w_{J_A}.$

Hence the pressure increment due to the addition of forward speed to the intake acting alone,

$$\Delta p_A = p_{A_{JV}} - p_{A_J} = p_{A_V} - \rho u_{V_A}u_{J_A} - \rho v_{V_A}v_{J_A} - \rho w_{V_A}w_{J_A}.$$

Similarly for point B (Fig. 2)

$$\Delta p_B = p_{B_{JV}} - p_{B_J} = p_{B_V} - \rho u_{V_B} u_{J_B} - \rho v_{V_B} v_{J_B} - \rho w_{V_B} w_{J_B}$$

but for the symmetry implied in Fig. 30,

$$u_{V_B} = u_{V_A} \qquad u_{J_B} = -u_{J_A} \quad \text{therefore } u_{V_B} u_{J_B} = -u_{V_A} u_{J_A}$$

$$v_{V_B} = -v_{V_A} \qquad v_{J_B} = v_{J_A} \quad \text{therefore } v_{V_B} v_{J_B} = -v_{V_A} v_{J_A}$$

$$w_{V_B} = -w_{V_A} \qquad w_{J_B} = w_{J_A} \quad \text{therefore } w_{J_B} w_{J_B} = -w_{J_A} w_{J_A}$$

so that

$$\Delta p_B = p_{B_V} + \rho u_{V_A} u_{J_A} + \rho v_{V_A} v_{J_A} + \rho w_{V_A} w_{J_A} = -\Delta p_A, \text{ since } p_{A_V} = p_{B_V},$$

i.e. the depression at F caused by the addition of the free stream to the intake acting alone equals the rise in pressure at B. It follows that the net lifting force on symmetrically disposed elements will be equal to that uf the fan acting alone.

Therefore, at forward speed V, Shroud Force $= \frac{1}{2}\rho V_J^2 A_J$. (4)

Notice that the argument concerning the additional force at forward speed rests only upon the assumptions of fore and aft symmetry (sideways symmetry not required) and of the validity of superposition. The expression for the force in the absence of free stream relies on the assumptions mentioned in the previous section.

Finally, combining (1) and (4) and introducing a coefficient k, based on mean dynamic head at the fan, which may take into account both diffusion and the drag of obstructions in the duct, we obtain

$$\text{Normal Force } N = A_J \Delta H + (1-k)\tfrac{1}{2}\rho \overline{V_J^2} A_J. \tag{5}$$

It may be convenient to determine the value of k from flow and force measurements at zero forward speed. Provided k is not too large this value will probably suffice at forward speed as well.

8.4 *Drag and Pitching Moment at Forward Speed*

Although the forces due to incremental induced pressures cancel out for lift there results a nose-up pitching moment which will be proportional to the product of forward speed and duct velocity and which depends upon model geometry. Similarly, induced pressures of opposite sense which act on forward and rearward facing areas respectively (on the duct walls in particular) will produce both pitching moment and drag. This is how both the momentum drag and the moment which turns the air into the duct are experienced by the shroud.

8.5. *Extension to Multiple Intakes*

The condition of symmetry that is now required is that the ducts shall be symmetrically disposed about a transverse line and that flows through mirrored pairs shall be equal. The effect of one such pair is considered in Fig. 3. As before no assumption is needed about the magnitude or direction of the velocities induced by the duct flows except that they are symmetrical about the y axis. Fig. 3 shows that the resultants induced by z and z' are also symmetrical in this way. The addition of velocities induced by other ducts does not alter this and components due to mainstream have the same effects as before.

9. *Application to Fan Systems*

The theoretical lift on the fan/straightener combination has been obtained in terms of the total-head rise across it and the lift on the shroud has been determined for a given duct velocity. The relationship between total-head rise and flow quantity, needed to complete the analysis, is a function of both fan geometry and, possibly to a lesser extent, scale. The slope of the characteristic total-head-rise curve, the dominant quantity, can differ quite widely between various wind-tunnel models and between model and full scale. This could be important if accurate comparisons are to be made.

As a first approximation the exit static pressure will be assumed to be atmospheric. Later it will be seen that the arguments which follow remain valid when exit conditions are affected by the interaction between the jet plume and the mainstream.

Consider two extreme shapes of fan characteristic total-head-rise curve based on tip-speed parameters. For a characteristic which is horizontal the pressure difference across the fan is constant. At a given fan rotational speed the throughput adjusts itself so that the jet dynamic pressure is increased above the value without forward velocity, by an amount equal to the free-stream dynamic pressure. Although the fan thrust is constant, the lift force on the shroud will increase.

On the other hand, when the fan characteristic is vertical, there is no change in jet flow rate as forward speed is increased and the increased inlet total head is felt as an increase in static pressure ahead of the fan. The fan thrust is reduced as forward speed rises, while the shroud force remains constant.

The broken lines in Fig. 32 show the variation of incremental lift with forward speed for the two idealised units mentioned above exhausting to ambient static pressure. Allowance has been made for a combination of diffusion in the duct behind the fan with losses due to the drag of items in the duct, using data from experiments described below. One third of the loss shown was brought about by the presence of traverse rakes in the duct. A relatively large drive shaft was also present. In the absence of diffusion and losses the fan and shroud lift would be equal at zero forward speed in both cases.

The chain dotted lines show the effect of inserting measured values of mean static pressure downstream of the fan into the calculation. It can be seen that while exit effects reduce the lift on the unit with the vertical characteristic, the lift for the horizontal characteristic is augmented since the exit suction increases the flow through the fan and hence the shroud lift. It is clear that a fan system whose total-head rise falls only slowly with increasing mass flow might be capable of producing additional lift force at constant rotational speed, at least partially to compensate for exit interference as forward speed increases. This would be accompanied by an increase in momentum drag. It is possible that an increased fan rotational speed from the static value in order to compensate for lift loss at forward speed may not be permissible for reasons of noise or the tip Mach number limitation.

It is difficult to see how the slope of the total-head-rise characteristic of a fan can be decreased without alteration to geometry as mass flow increases. Variable pitch could be used to give a characteristic which effectively has a zero or even a positive slope, which is unstable for fixed geometry devices but in the interests of simplicity fixed geometry is clearly desirable. Although the slope of the characteristic is reduced as a fan approaches the stall, any solution using this effect would be artificial since static lift would be capable of improvement. A fan or blower is needed whose elements are insensitive to incidence.

Finally, having established that the idealised unit with the horizontal characteristic is capable of lift increases at forward speed we shall examine the power output of the fan and the power required to overcome momentum drag.

As might be expected the unit with the horizontal characteristic requires more power than the unit with the vertical one (Fig. 33). Lift power is relatively greater both because the total-head rise does not decrease and because the mass flow increases with forward speed. The power to overcome momentum drag is also relatively greater for this reason.

However, when the results of Figs. 32 and 33 are combined to produce figures of merit, plotted in Fig. 34 it can be seen that the performance of both units is similar. The figures of merit for the lifting part of the power required by the two units were found to be so close as to be indistinguishable in the diagram, while the unit with the horizontal characteristic is marginally better when momentum drag is included.

The reason is that the power to overcome momentum drag is a smaller proportion of the total power required by the unit with the horizontal characteristic.

We conclude that extra lift is available at forward speed from the unit with the horizontal characteristic, without increase of rotational speed, at a figure of merit (based on output power) similar to the unit with the vertical characteristic. It is also worthy of note that much of the extra power required by the unit with the horizontal characteristic might be supplied by a thrust engine installed for cruise, used to overcome momentum drag.

10. *Fan Interaction and Total Lift Loss for the Streamlined Nacelle Wind-Tunnel Model.*

The results of the experiments described in Part I will now be examined in the light of the above analysis. The model was specifically designed so that a minimum horizontal area around the jet was exposed to strong suctions there, consistent with a streamlined shape. Thus with the exception of models truncated behind the jet this model form is the one for which fan interaction forces should form the most noticeable proportion of the incremental-lift loss at forward speed.

Figs. 35 and 36 are derived from flow measurements at a plane between the fan and straighteners. The upper part of Fig. 35 is indicative of the variation of conditions at the duct inlet and outlet with forward speed but since these curves were derived from measurements behind the fan no scale has been given. The upper curve shows that the static pressure at inlet rises with forward speed as would be expected from previous arguments. This rise is less than the dynamic head of the forward stream because of the slight increase in jet velocity. In Fig. 35, (4) is the inlet static pressure which would result if the jet velocity was unchanged by changes in the pressure difference across the fan, i.e. if the total-head-rise characteristic was vertical.

(2) is the measured static pressure in the swirled flow at the traverse plane. There was some correlation between these static pressures and measured lift increments. In calculating the pressure rise through the straighteners to obtain curve (3) allowance has been made for the decrease in swirl as the fan moves down its characteristic curve.

In the lower part of Fig. 35 the progression of the fan down its characteristic is plotted conventionally. The difference between the experimental points and the calculated curve probably combines the effects of fan manufacturing errors with those of cross flow. However, it can be seen that a reasonably accurate prediction can be made of the change of jet velocity with forward speed if freestream static pressure is assumed at exit.

Fig. 36 shows the result of analysing the above data using the expressions obtained in Section 9, suitably modified to allow for losses. Though there is a decrease in total lift with forward speed the effect is much less pronounced than for the vertical characteristic of Fig. 22. Incremental lift results at positive incidences should be considered with care, since tunnel interference effects were probably present.

Fig. 37 is a comparison between the measured drag increments and values calculated from duct flow measurements. The latter comprise the drag due to the removal of free-stream momentum from the measured mass flow plus the streamwise component of the normal force N, calculated from equation (5).

It can be seen that the differences between the measured and the calculated incremental-drag values are of the same order as those for incremental lift (Fig. 26). The suctions on the sloping surfaces behind the jet probably contribute both to lift and drag interference effects. However, it seems likely that the variations of static pressure on the duct walls has a more significant effect on drag than on lift increments.

Fig. 37 also shows that estimated drag increments based on the nominal efflux velocity V_{J_T} can be considerably in error. A better estimate is given by measured values of mass flow. Failing this, estimates based on the operating points predicted as in Fig. 35 are to be preferred to those based on V_{J_T}. Note should also be taken of the increase in drag due to tunnel constraint, illustrated for $\alpha = +12$ deg in Fig 10 (*see* also Ref. 3 and Part I).

In order to put all of the above into correct perspective so far as lift force and performance are concerned the changes of lift due to fan interaction will now be compared with the overall loss of lift increment at the lower forward speeds. This is done for several incidences in Fig. 26. The effect of incidence

on the fan interaction is small (*see* Fig. 11 and Ref. 1). The second and fourth diagrams show that while for the plain body the fan-interaction incremental-lift loss can amount to about half of the total loss, the addition of underfins has a much more significant effect.

11.1. *Conclusions (Part I).*

(1) By designing for a low horizontal area around the jet exit the maximum loss of lift on a streamlined body at forward speed has been reduced to about 10 per cent at zero incidence. The addition of wings increased the loss but underfins almost eliminated it.

(2) Up to half of the loss of lift could be attributed to the fan and intake combination, rather than jet exit effects.

(3) The intake design would have benefited from larger lip radii 45° each side of the forward centreline. On the present model a lip radius of one fifth of the duct diameter on the upstream side of the intake decreased linearly with angle to 6 per cent at the 90° positions. The highest forward speed was 65 per cent of that of the jet.

(4) As a result of surface flow observations on the sides of the body it is thought that, within the limited speed range considered, the movement of the jet plume towards the body is accompanied by a complementary reduction in the strength of the trailing vortices within the plume.

(5) About half the difference between measured drag increments and estimates based on nominal efflux velocity results from the increase of mass flow through the fan with forward speed. The remainder of the increase probably includes drag due to suctions immediately behind the jet, which also reduce lift.

(6) With the exception of cases with the wing stalled, the drag increments measured in the larger tunnel were equal for all configurations of the model.

(7) The chief drawback of upper-surface intakes is probably the large increase in nose-up pitching moment, proportional to forward speed. A control jet, placed 4 main jet diameters behind the jet would require a thrust of 20 per cent total lift at V/V_J of 0·4, a high transition speed.

(8) If the plain body is regarded as a pylon-mounted lifting nacelle, then the pitching moment problem could be resolved by placing the duct transversely, or alleviated by placing the inlet plane at an altitude slightly below that of the centre of gravity of the aircraft.

Tunnel interference

(9) With the 5 ft × 4 ft tunnel closed the static lift was 7 per cent below that obtained after cutting a hole in the tunnel floor to allow the jet to escape and opening all possible doors and windows. The tunnel floor was 3·2 diameters below the jet exit.

(10) Floor stagnation occurred below the model in the 5 ft × 4 ft wind tunnel below velocity ratios V/V_J ranging from 0·20 at −20 deg incidence to 0·40 at +20 deg.

A comparison of forces measured in the 5 ft × 4 ft and in the $11\frac{1}{2}$ ft × $8\frac{1}{2}$ ft tunnels yielded the following results:

(11) With the plain body at 18 deg incidence an apparent lift benefit in the smaller tunnel increased with forward speed to 10 per cent of static lift at a velocity ratio of 0·60. Somewhat surprisingly this high incidence effect disappeared when underfins were added. At lower incidences lift increments agreed to within ±2 per cent.

(12) With wings added the lift increment recovered, after the initial fall, at a lower forward speed in the smaller tunnel. This gave an apparent lift benefit which rose from 3 per cent at one third of the jet velocity to 15 per cent at a velocity ratio of 0·60. The above differences are important because results tend to be optimistic if the tunnel is too small.

(13) The above apparent lift benefits in the smaller tunnel were usually accompanied by correspondingly greater drag and pitching-moment increments.

11.2. *Conclusions (Part II)*

It has been possible to determine the effect of a simple fan-mainstream interaction on forces on a lifting unit using only a single major assumption concerning fore and aft symmetry about a transverse

line across a wing or body which contains a lifting unit or units. For multi-engined lifting pods in particular the assumption is not too restrictive since in most cases in which lift loss is likely to be embarrassing all engines will pass approximately the same mass flow, the maximum, and may have reached a limiting tip Mach number, thus preserving fore and aft symmetry.

It has been shown that for the wind-tunnel model described in Part I used here as an example, the loss of lift due to fan-mainstream interaction, though amounting in some cases to half of the lift loss at forward speed, amounted to no more than 5 per cent, an amount readily recoverable by the use of underfins, for example.

However, it is thought that the chief use of the analysis presented here is likely to be in making comparisons either between wind-tunnel models containing fans of differing geometries, or with full-scale fans or engines for which both geometry and Reynolds number are likely to differ markedly from the corresponding tunnel model. As an example of differences between model fans, the slope of the total-head characteristic curve for the model fan used here as an example was only two thirds of that for the fan described in Ref. 6. Models containing the latter fan might therefore be expected to experience correspondingly less interference force due to fan-mainstream interaction, assuming losses to be the same in both cases.

By examining the lift on an idealised theoretical unit having first a vertical and then a horizontal characteristic total-head-rise curve based on tip-speed parameters, the benefits of using a constant pressure-rise lifting unit have been demonstrated. Such a unit could be particularly useful for wing installation since any depression of exit static pressure, due to plume interference, would be transferred by the fan to the inlet and over the upper surface. Useful alleviation of lift loss might result.

However, it is not easy to see how the slope of the total-head-rise characteristic curve can be changed for a conventional fan with fixed geometry, which is clearly desirable. Variable pitch could be used to give a characteristic which effectively has a positive slope, which is unstable for fixed geometry devices. Although the slope of the characteristics of a fixed geometry fan decreases as the blades stall any solution using this effect would be artificial since static lift would be capable of improvement. A fan or blower is needed whose elements are insensitive to incidence.

9. *Acknowledgements*

The author is indebted to the late Professor H. B. Squire, who suggested the project, for advice and encouragement during the early stages of the work. The author also had valuable discussions with Dr. J. Williams and Dr. L. A. Wyatt at R.A.E. and Mr. N. Gregory of N.P.L.

The model was made at Imperial College by Mr. R. A. Lee and the photography was by Mr. J. P. O'Leary. The work was the subject of a research contract between the Ministry of Aviation and the Imperial College of Science and Technology.

LIST OF SYMBOLS

A_J	Fan annular area
C_L	Lift coefficient
C_D	Drag coefficient
C_m	Nose-up pitching-moment coefficient measured about the axis of suspension of the model
ΔC_p	Defined in Fig. 9
D	Drag
ΔD	Drag increment due to fan operation (datum with duct ends sealed)
d	Fan tip diameter
$\overline{H}$	Mean total head at central plane, measured above ambient static pressure
ΔH	Net total-head rise through fan and straighteners
k	*See* equation (5)
L	Lift
ΔL	Lift increment due to fan operation (datum with duct ends sealed)
M	Pitching moment, positive nose up
ΔM	Nose-up pitching-moment increment due to fan operation (datum with duct ends sealed)
M_T	Fan tip peripheral Mach number
N	Body normal force as determined in equation (5)
p	Static pressure
p_0	Static pressure at infinity (zero forward speed cases)
	Static pressure in the free stream
Δp	Change in surface static pressure due to the addition of the free stream to an intake acting alone (*see* Section 8·3)
P_I	Electrical power input to motor
P_{I_T}	Electrical power input to motor during static-lift test
q_v, q_j, q_{V_J}	*See* Section 8·3
R	Fan tip radius
r	Radius of fan blade element
T	Measured static lift
u, v, w	*See* Section 8·3
V	Free-stream velocity

V_J	Jet velocity (in fan annulus)
V_{J_T}	Nominal efflux velocity defined by $T = \rho A_J V_{J_T}^2$
$V_{J_{rms}}$	Root mean square jet velocity
α	Body incidence
α_o	Wing setting angle; positive for wing leading edge above the body axis
α_w	Wing incidence
Λ	Fan advance ratio $V_J/\Omega R$
ρ	Air density
θ, Θ	*See* Fig. 29
ξ	Bendemann figure of merit
Ω	Angular velocity of fan

REFERENCES

No.	Author(s)	Title, etc.
1	J. E. Hackett	Some preliminary results of force tests on a fan-lift model Imperial College Department of Aeronautics TN 20, March, 1962.
2	W. J. G. Trebble and J. E. Hackett	Low-speed wind tunnel tests on a streamlined body containing a ducted lifting fan. R.A.E. T.N. Aero 2893, May, 1963. A.R.C. 25084.
3	J. E. Hackett	Wind tunnel tests on an aircraft model with a lifting fan unit installed in the body. London University Ph.D. Thesis, March, 1964.
4	U. W. Schaub and E. P. Cockshutt	Analytic and experimental studies of normal inlets, with special reference to fan-in-wing VTOL power plants. ICAS Paper No. 64–572, 1964.
5	W. J. G. Trebble J. Williams	Exploratory wind-tunnel investigations of a bluff body containing a lifting fan. A.R.C. C.P. No. 597, April, 1961.
6	N. Gregory, W. G. Raymer and Edna M. Love	The effect of forward speed on the inlet flow distribution and performance of a lifting fan installed in a wing. A.R.C. R. & M. 3388, June, 1962.
7	N. Gregory and W. G. Raymer	Wind tunnel tests on the Boulton Paul rectangular wing (aspect ratio 2) with lifting fan. Series I, A.R.C.20 356, August, 1958. Series II, A.R.C.21 127, July, 1959.
8	L. A. Wyatt	Preliminary note on a wind tunnel test of a wing fitted with multiple lifting fans. A.R.C.21 377, October, 1959.
9	W. H. Melbourne	Experiments on a delta wing with jet-assisted lift. A.R.C.R. & M.3288, May, 1960.
10	L. A. Wyatt	Unpublished M.O.A.work.
11	N. Gregory and Edna M. Love	Wind tunnel tests on a nacelle fitted with two lifting fans in tandem. A.R.C. R. & M. 3494, January 1966.
12	J. E. Hackett	Report to be published.
13	B. Thwaites	*Incompressible Aerodynamics*, pp. 415–417. Oxford University Press, 1960.
14	I. A. Abbott and A. E. Von Doenhoff	*Theory of Wing Sections*, p. 16. Dover Publications Inc., 1959.
15	S. Goldstein (Ed.)	*Modern Developments in Fluid Dynamics*, p. 508. Oxford University Press, 1938.
16	R. A. Wallis	Axial Flow Fans, p. 293. Newnes, 1961.
17	R. Jordinson	Flow in a jet directed normal to the wind. A.R.C. R. & M. 3074, October, 1956.

No.	*Author(s)*	*Title, etc.*
18	L. J. S. Bradbury and M. N. Wood	The static pressure distribution around a circular jet exhausting normally from a plane wall into an airstream. R.A.E. T.N. Aero.2978, August, 1964.
19	J. E. Hackett	Wind tunnel tests on a streamlined fan-lift nacelle, alone and with wings or underfins fitted. A.R.C. 26 969, May, 1965.
20	J. E. Hackett	The effect of forward speed on the lift produced by a lifting fan and its inlet. A.R.C. 27 330, October, 1965.

Table 1

Model Dimensions

Body	
Length	40·5 in.
Maximum width	9·0 in.
Maximum depth	8·0 in.
Maximum cross-sectional area	0·46 sq ft
Distance from nose to wing quarter chord	16·4 in. (= 40% body length)
Distance from nose to duct axis (which is at right-angles to the body centreline)	16·4 in.
Duct and Centrebody	
Duct length	8·0 in.
Duct diameter (= d)	6·4 in.
Distance from inlet to fan plane	2·25 in.
Annular area of duct ($7\frac{1}{2}$% of wing area)	0·15 sq ft
Distance from inlet to straighteners	6·0 in.
Inlet radius on upstream side of duct (= 20%d)	1·3 in.
Inlet radius on downstream side of duct (= 6%d)	0·38 in.
No radius on duct outlet	
Centrebody length	9·0 in.
Maximum centrebody diameter	3·7 in.
Length of cylindrical portion of centrebody (ends are ellipsoidal)	3·0 in.
Fan and Straighteners	
Tip diameter (= d)	6·4 in.
Boss diameter (= 58%d)	3·7 in.
Fan	
5 Blades 10% Clark Y section	
Root blade angle	$32\frac{1}{2}°$
Tip blade angle	$17\frac{1}{2}°$
Root chord	1·10 in.
Tip chord	0·95 in.
Straighteners	
12 Blades, thin cambered plates	
Blade chord	1·3 in.
Wing	
Span	34·0 in.
Area	2·0 sq ft
Aspect ratio	6·0
Taper ratio	2·0
Unswept quarter chord	
Aerofoil section	NACA 0012
Wing-body angle adjustment range	±30°
Struts	
Diameter	1·0 in.
Distance between outer ends	29·0 in.
Distance from nose of body	16·4 in.

TABLE 2

Summary of Tests

1.

Wind Tunnel and Test Date	Imperial College 5 ft × 4 ft. Late 1961
Configurations	Plain body, body with wings (without underfins)
Variables	V, 30 ft/sec to 130 ft/sec. 20 ft/sec intervals $\alpha = -20°, -18°$, to $+18°, +20°$. 3° intervals α_0, $-10°$ to $+20°$. 5° intervals, consistent with $\lvert\alpha_W\rvert < 20°$
Measurements and Tests	Lift, drag and pitching moment Surface flow visualization Determination of floor stagnation regime Pitot-static traverse at duct exit in the static-lift condition

2.

Wind Tunnel and Test Date	Royal Aircraft Establishment $11\frac{1}{2}$ ft × $8\frac{1}{2}$ ft, No. 1. June, 1962.
Configurations	Plain body, body with wings, with and without underfins
Variables	V, 20 ft/sec to 80 ft/sec and 120 ft/sec. 20 ft/sec intervals α, $-18°$ to $+18°$. 6° intervals $\alpha_0 = 0°$
Measurements	Lift, drag and pitching moment

3.

Wind Tunnel and Test Date	Imperial College 5 ft × 4 ft. October, 1962
Configurations	Plain body, with and without underfins
Variables	V, 30 ft/sec to 110 ft/sec, 20 ft/sec intervals α, $-18°$ to $+18°$. 6° intervals.
Measurements and Tests	Lift, drag and pitching moment Electrical power input Fan r.p.m. Duct flow measurements } Simultaneously (Series 3a) Flow visualization on fins Check force tests with pressure tubes disconnected (Series 3b)

TABLE 3

Force Tests in Two Wind Tunnels.

(A) Plain Body.

		Test Series 3b (5 ft × 4 ft *Tunnel*)			*Test Series* 2 (11½ ft × 8½ ft *Tunnel*)		
$V/\Omega R$	$\alpha°$	(1)*	(2)	(3)	(1)	(2)	(3)
0·030	−18				0·0860	−0·0180	0·0084
	−12				0·0880	−0·0096	0·0075
	−6				0·0914	−0·0010	0·0098
	0				0·0908	+0·0100	0·0084
	6				0·0889	0·0174	0·0112
	12				0·0872	0·0280	0·0055
	18				0·0835	0·0370	0·0075
0·060	−18	0·0879	−0·0058	0·0252	0·0872	−0·0063	0·0255
	−12	0·0883	+0·0038	0·0260	0·0895	+0·0023	0·0216
	−6	0·0886	0·0135	0·0328	0·0900	0·0108	0·0241
	0	0·0880	0·0226	0·0296	0·0900	0·0220	0·0255
	6	0·0849	0·0335	0·0300	0·0860	0·0302	0·0260
	12	0·0814	0·0430	0·0372	0·0840	0·0386	0·0220
	18	0·0795	0·0520	0·0355	0·0818	0·0472	0·0255
0·090	−18	0·0788	0·0060	0·0420	0·0894	0·0050	0·0442
	−12	0·0874	0·0152	0·0425	0·0883	0·0140	0·0400
	−6	0·0864	0·0245	0·0504	0·0875	0·0235	0·0440
	0	0·0851	0·0342	0·0504	0·0849	0·0350	0·0478
	6	0·0813	0·0440	0·0504	0·0819	0·0420	0·0460
	12	0·0795	0·0522	0·0600	0·0793	0·0500	0·0422
	18	0·0803	0·0640	0·0580	0·0810	0·0595	0·0470
0·120	−18	0·0903	0·0170	0·0598	0·0920	0·0163	0·0644
	−12	0·0860	0·0268	0·0642	0·0891	0·0258	0·0597
	−6	0·0850	0·0360	0·0704	0·0853	0·0352	0·0632
	0	0·0835	0·0462	0·0720	0·0798	0·0448	0·0698
	6	0·0799	0·0444	0·0726	0·0791	0·0533	0·0670
	12	0·0788	0·0632	0·0830	0·0786	0·0615	0·0630
	18	0·0820	0·0783	0·0808	0·0790	0·0700	0·0666
0·150	−18	0·0924	0·0283	0·0786			
	−12	0·0860	0·0283	0·0844			
	−6	0·0865	0·0472	0·0920			
	0	0·0832	0·0580	0·0942			
	6	0·0781	0·0655	0·0963			
	12	0·0780	0·0754	0·1052			
	18	0·0860	0·0945	0·1038			
0·180	−18	0·0957	0·0418	0·1038	0·0971	0·0404	0·1042
	−12	0·0904	0·0517	0·1050	0·0908	0·0498	0·0982
	−6	0·0890	0·0597		0·0870	0·0594	0·1037
	0	0·0840	0·0709	0·1160	0·0830	0·0688	0·1143
	6	0·0769	0·0789	0·1240	0·0813	0·0785	0·1180
	12	0·0779	0·0912	0·1320	0·0789	0·0820	0·1203
	18	0·0902	0·1130	0·1280	0·0801	0·0955	0·1167

See Conclusion of Table 3 for footnotes.

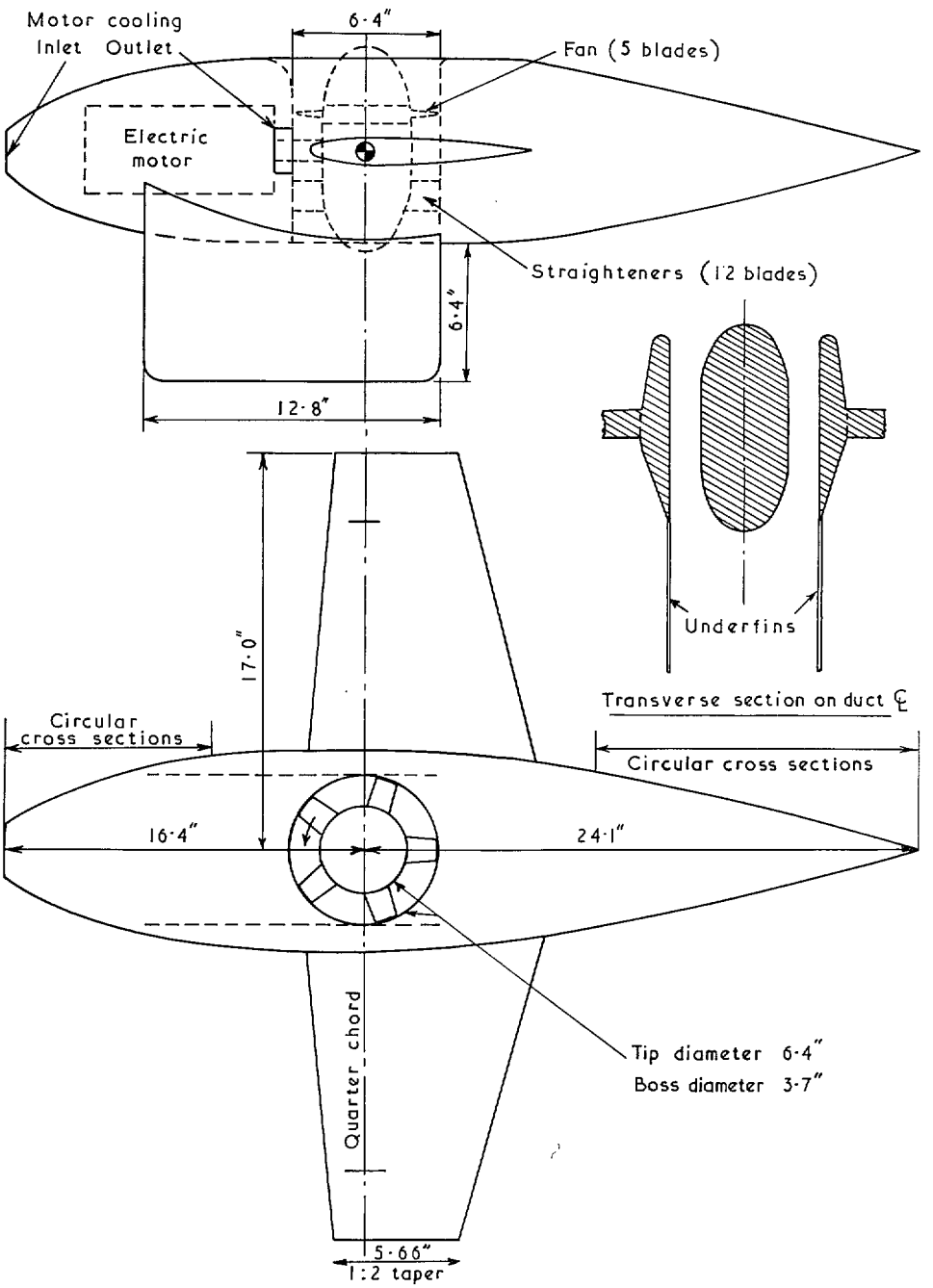

FIG. 1. General arrangement of model

TABLE 3 (*contd.*)

(*D*) *Body with Wings and Fins*[+]

		(5 ft × 4 ft *Tunnel*)			*Test Series* 2 ($11\frac{1}{2}$ ft × $8\frac{1}{2}$ ft *Tunnel*)		
$V/\Omega R$	$\alpha°$	(1)	(2)	(3)	(1)	(2)	(3)
0·030	−18				0·0842	−0·0180	0·0085
	−12				0·0876	−0·0080	0·0075
	−6				0·0892	+0·0007	0·0053
	0				0·0890	0·0117	0·0130
	6				0·0876	0·0208	0·0115
	12				0·0876	0·0290	0·0095
	18				0·0840	0·0369	0·0097
0·060	−18				0·0754	−0·0080	0·0220
	−12				0·0822	0·0047	0·0260
	−6				0·0852	0·0120	0·0280
	0				0·0840	0·0215	0·0317
	6				0·0834	0·0303	0·0284
	12				0·0830	0·0370	0·0317
	18				0·0820	0·0442	0·0273
0·090	−18				0·0672	−0·0008	0·0360
	−12				0·0878	0·0140	0·0475
	−6				0·0882	0·0234	0·0530
	0				0·0890	0·0320	0·0530
	6				0·0870	0·0409	0·0530
	12				0·0880	0·0470	0·0547
	18				0·0850	0·0520	0·0467
0·120	−18				0·0602	0·0043	0·0520
	−12				0·0940	0·0250	0·0740
	−6				0·0934	0·0349	0·0750
	0				0·0904	0·0434	0·0762
	6				0·0870	0·0515	0·0760
	12				0·0950	0·0584	0·0730
	18				0·0904	0·0608	0·0710
0·150	−18						
	−12						
	−6						
	0						
	6						
	12						
	18						
0·180	−18				0·0480	0·0124	0·0940
	−12				0·1056	0·0483	0·1240
	−6				0·1060	0·0580	0·1320
	0				0·1070	0·0660	0·1280
	6				0·1040	0·0760	0·1238
	12				0·1126	0·0845	0·1210
	18				0·1112	0·0808	0·1078

NO TESTS PERFORMED

$$(1) = \frac{\Delta L}{\rho(\Omega R)^2 A_J} \qquad (2) = \frac{\Delta D}{\rho(\Omega R)^2 A_J} \qquad (3) = \frac{\Delta M}{\rho(\Omega R)^2 A_J d}$$

Values shown obtained as cross-plots. * Including 3 per cent correction for drag of traverse rakes.

[+] Δ increments are measured above a datum with fins.

TABLE 3 (*contd.*)

(*C*) *Plain Body with Fins*[+]

		Test Series 3b (5 ft × 4 ft *Tunnel*)			*Test Series* 2 ($11\frac{1}{2}$ ft × $8\frac{1}{2}$ ft *Tunnel*)		
$V/\Omega R$	$\alpha°$	(1)*	(2)	(3)	(1)	(2)	(3)
0·030	−18						
	−12						
	−6						
	0	NO TESTS PERFORMED					
	6						
	12						
	18						
0·060	−18	0·0859	−0·0070	0·0290			
	−12	0·0893	0·0040	0·0312			
	−6	0·0895	0·0140	0·0322			
	0	0·0903	0·0237	0·0370			
	6	0·0883	0·0320	0·0355			
	12	0·0878	0·0416	0·0380			
	18	0·0834	0·0495	0·0360			
0·090	−18	0·0890	0·0018	0·0520	0·0914	0·0055	0·0490
	−12	0·0930	0·0142	0·0540	0·0915	0·0143	0·0520
	−6	0·0923	0·0244	0·0563	0·0929	0·0227	0·0492
	0	0·0947	0·0339	0·0585	0·0914	0·0340	0·0470
	6	0·0912	0·0420	0·0580	0·0918	0·0407	0·0483
	12	0·0893	0·0550	0·0564	0·0899	0·0468	0·0482
	18	0·0863	0·0559	0·0509	0·0834	0·0532	0·0420
0·120	−18	0·0949	0·0150	0·0755	0·0986	0·0160	0·0710
	−12	0·0995	0·0249	0·0790	0·0987	0·0253	0·0750
	−6	0·0982	0·0350	0·0805	0·0982	0·0340	0·0800
	0	0·1034	0·0440	0·0810	0·0985	0·0440	0·0820
	6	0·0969	0·0522	0·0759	0·0973	0·0520	0·0790
	12	0·0932	0·0600	0·0738	0·0946	0·0593	0·0740
	18	0·0907	0·0640	0·0660	0·0890	0·0660	0·0660
0·150	−18	0·1044	0·0249	0·1025			
	−12	0·1117	0·0350	0·1058			
	−6	0·1093	0·0463	0·1043			
	0	0·1150	0·0544	0·1043			
	6	0·1056	0·0622	0·0959			
	12	0·1024	0·0693	0·0920			
;	18	0·0982	0·0738	0·0820			
0·180	−18	0·1128	0·0320	0·1308		0·0367	0·1153
	−12	0·1262	0·0453	0·1373	0·1209	0·0470	0·1208
	−6	0·1236	0·0558	0·1300	0·1182	0·0574	0·1251
	0	0·1273	0·0650	0·1270	0·1170	0·0680	0·1365
	6	0·1150	0·0725	0·1190	0·1150	0·0770	0·1280
	12	0·1130	0·0792	0·1113	0·1116	0·0842	0·1200
	18	0·1100	0·0836	0·1000	0·1042	0·0890	0·1100

See conclusion of Table 3 for footnotes.

TABLE 3 (*contd.*)

(*B*) *Body with Wings*

		Test Series 1 (5 ft × 4 ft *Tunnel*)			*Test Series* 2 ($11\frac{1}{2}$ ft × $8\frac{1}{2}$ ft *Tunnel*)		
$V/\Omega R$	$\alpha°$	(1)	(2)	(3)	(1)	(2)	(3)
0·030	−18				0·0878	−0·0183	−0·001
	−12				0·0900	−0·0083	+0·0060
	−6				0·0930	+0·0020	0·0030
	0				0·0930	0·0094	0·0102
	6				0·0930	0·0193	0·0049
	12				0·0918	0·0293	0·0160
	18				0·0895	0·0360	0·0184
0·060	−18	0·0792	−0·0078	0·0173	0·0780	−0·0085	0·0180
	−12	0·0852	+0·0080	0·0270	0·0832	+0·0039	0·0261
	−6	0·0840	+0·0163	0·0307	0·0838	0·0133	0·0292
	0	0·0830	0·0263	0·0342	0·0826	0·0215	0·0315
	6	0·0817	0·0340	0·0360	0·0806	0·0307	0·0260
	12	0·0830	0·0440	0·0360	0·0812	0·0392	0·0214
	18	0·0910	0·0522	0·0332	0·0826	0·0455	0·0260
0·090	−18	0·0680	0	0·0320	0·0640	−0·0008	0·0326
	−12	0·0838	0·0178	0·0470	0·0796	+0·0150	0·0462
	−6	0·0800	0·0270	0·0525	0·0790	0·0244	0·0539
	0	0·0782	0·0352	0·0562	0·0767	0·0335	0·0520
	6	0·0790	0·0432	0·0568	0·0750	0·0412	0·0490
	12	0·0790	0·0544	0·0523	0·0743	0·0490	0·0400
	18	0·0918	0·0619	0·0493	0·0795	0·0548	0·0433
0·120	−18	0·0558	0·0053	0·0459	0·0504	0·0055	0·0466
	−12	0·0850	0·0287	0·0686	0·0792	0·0255	0·0602
	−6	0·0862	0·0380	0·0748	0·0790	0·0350	0·0738
	0	0·0790	0·0458	0·0780	0·0750	0·0434	0·0740
	6	0·0790	0·0540	0·0762	0·0720	0·0520	0·0714
	12	0·0744	0·0669	0·0710	0·0728	0·0620	0·0640
	18	0·0920	0·0727	0·0690	0·0798	0·0634	0·0630
0·150	−18	0·0460	0·0090	0·0546			
	−12	0·0980	0·0388	0·0850			
	−6	0·0986	0·0489	0·0925			
	0	0·0948	0·0567	0·1029			
	6	0·0862	0·0660	0·0993			
	12	0·0718	0·0813	0·0905			
	18	0·0920	0·0840	0·0890			
0·180	−18	0·0368	0·0090	0·0620	0·0304	0·0140	0·0366
	−12	0·1145	0·0493	0·1032	0·1002	0·0463	0·0860
	−6	0·1107	0·0603	0·1172	0·0963	0·0573	0·0991
	0	0·1106	0·0670	0·1272	0·0890	0·0608	0·1202
	6	0·0932	0·0770	0·1260	0·0840	0·0698	0·1210
	12	0·0702	0·1000	0·1100	0·0837	0·0800	0·1140
	18	0·0912	0·0943	0·1100	0·0800	0·0793	0·1098

See conclusion of Table 3 for footnotes.

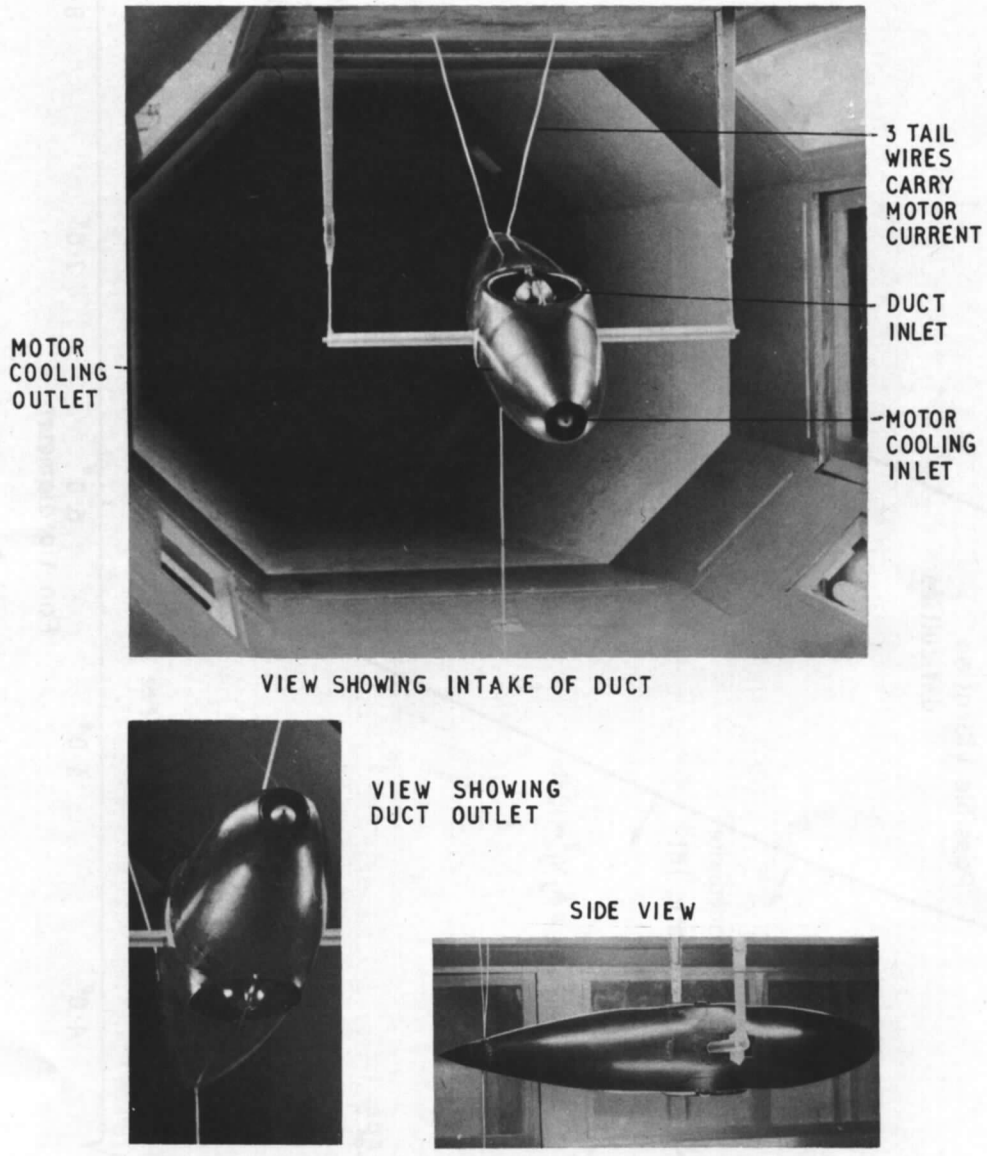

FIG. 2. General views of fan lift model 'plain body' configuration

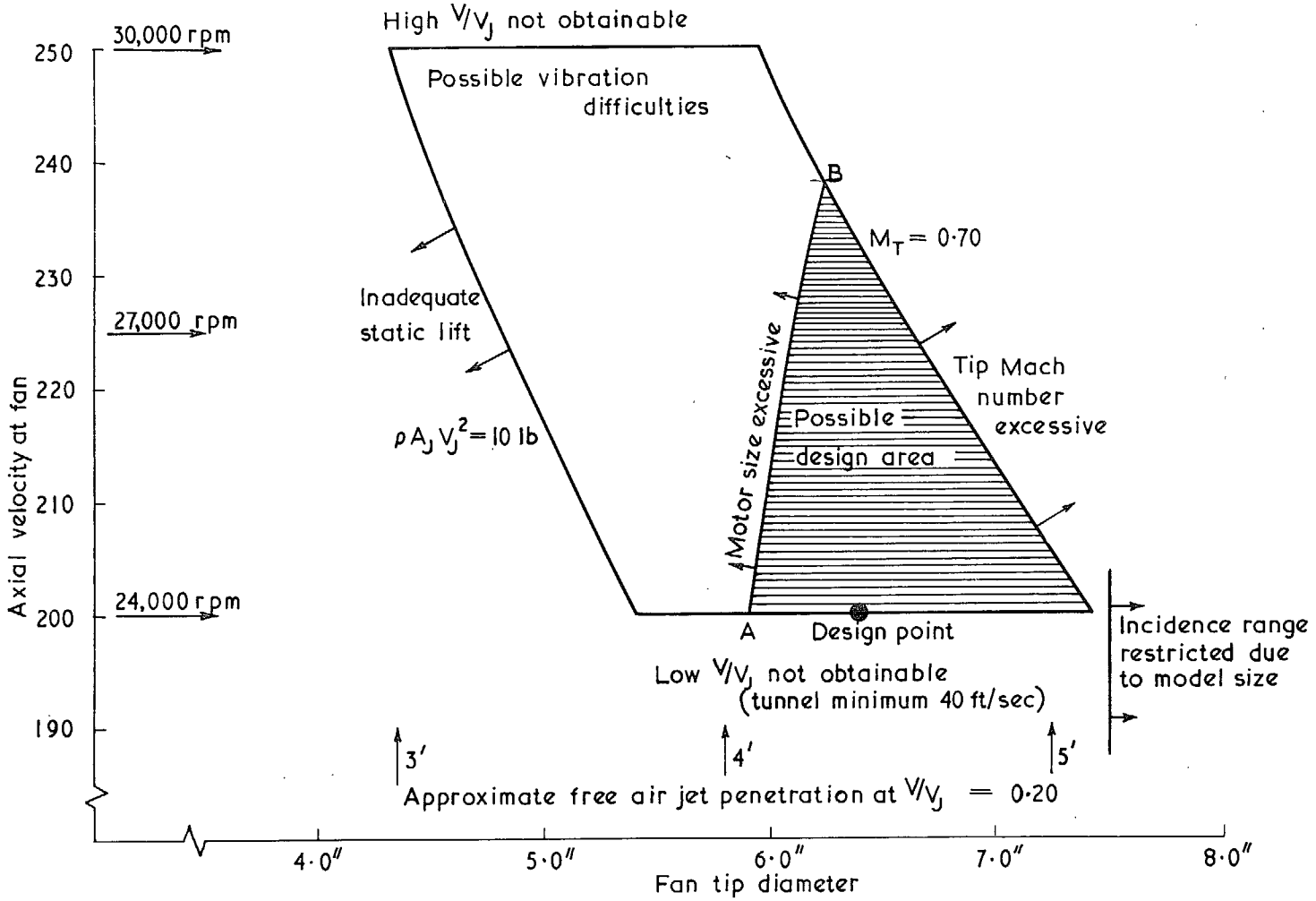

FIG. 3 Fan design boundaries

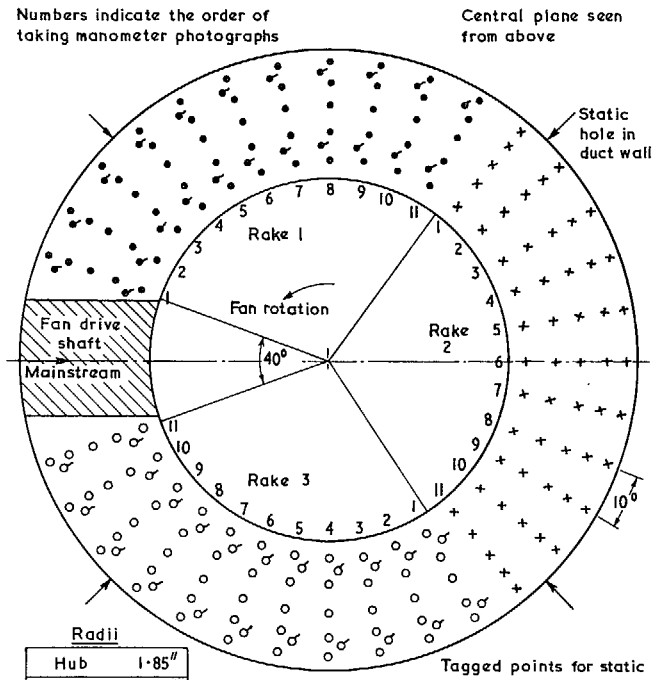

Radii

Hub	1·85″
Total tube	2·05″
Static tube	2·21″
Total tube	2·37″
Total tube	2·64″
Total tube	2·89″
Static tube	2·99″
Total tube	3·09″
Duct wall	3·20″

FIG. 4. Details of traverse positions (3 rakes).

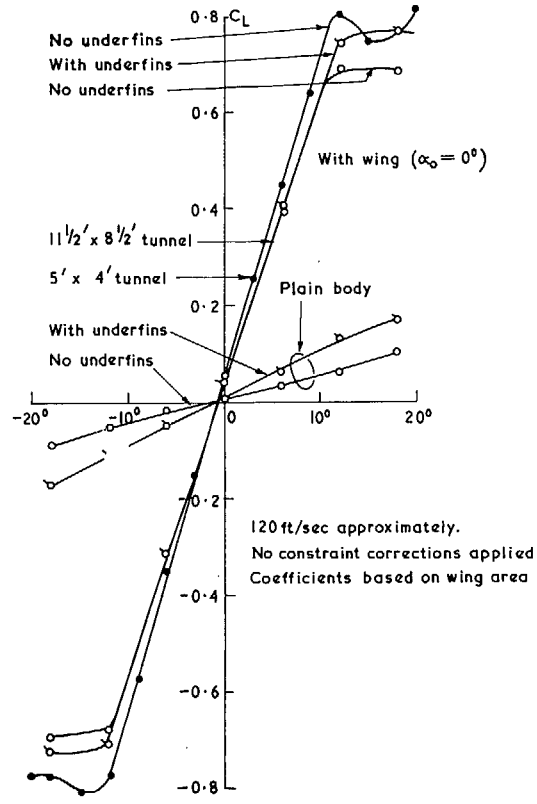

FIG. 5. Lift characteristics with the duct sealed at both ends

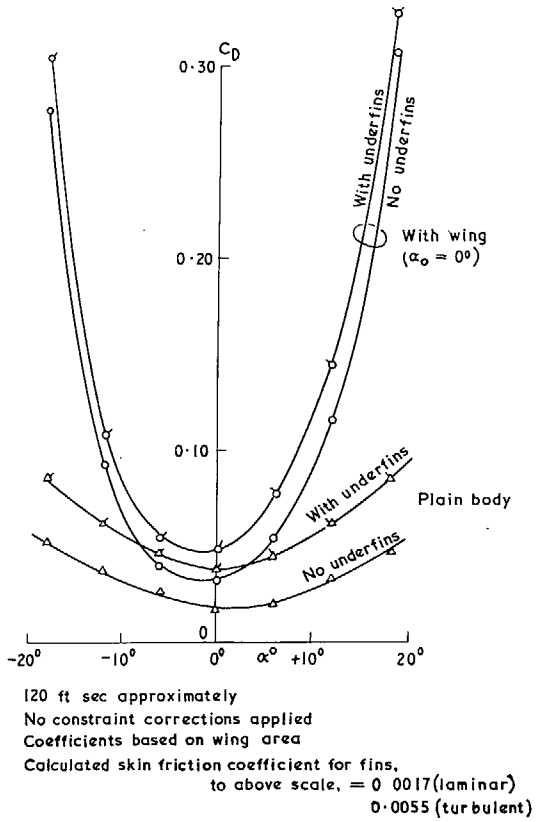

FIG. 6. Drag characteristics with the duct sealed at both ends

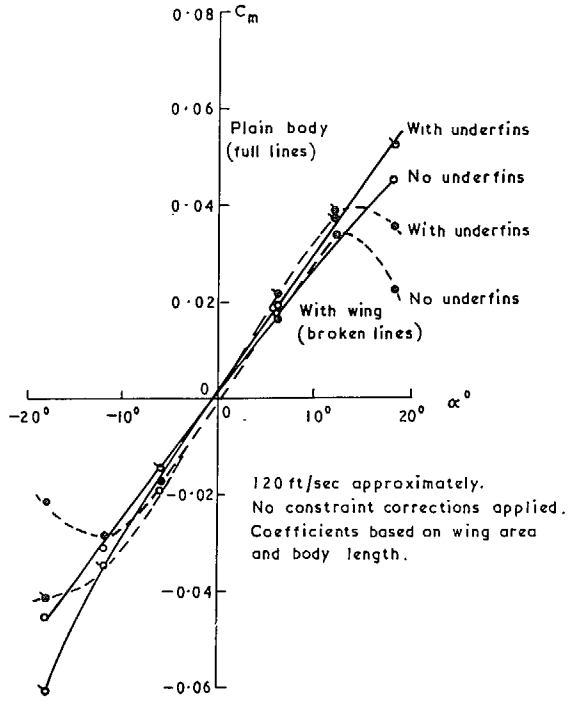

FIG. 7. Pitching-moment characteristics with duct sealed at both ends

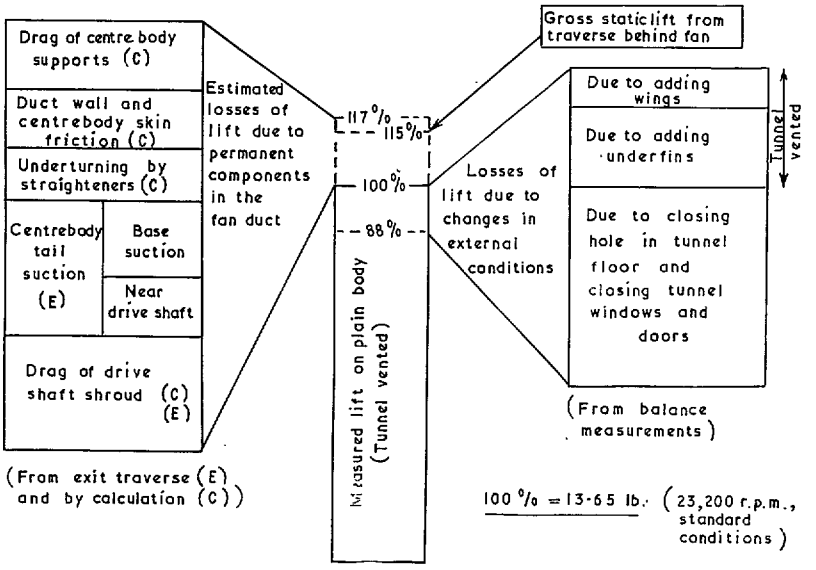

FIG. 8. Analysis of static-lift component parts
(Measurements made in 5 ft × 4 ft tunnel)

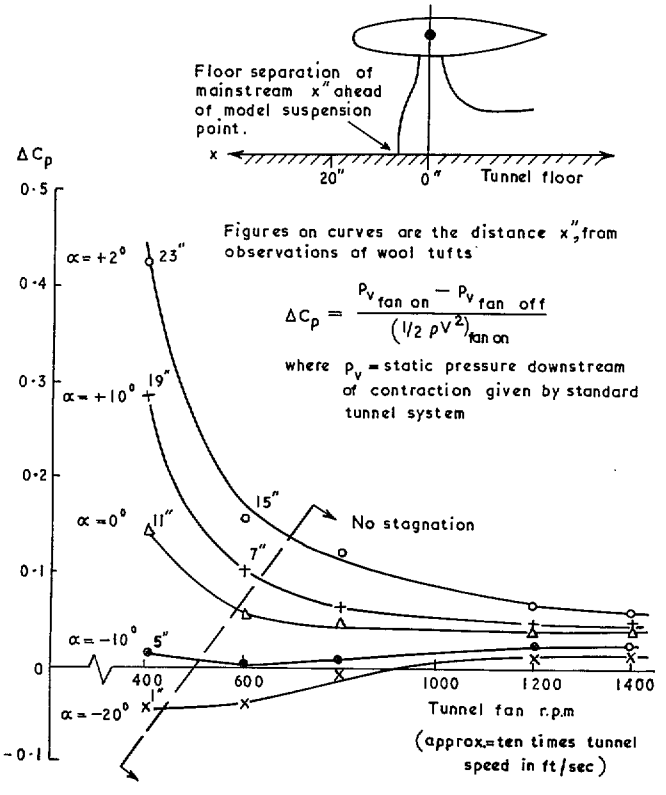

FIG. 9. The effects of fan operation on upstream static pressure

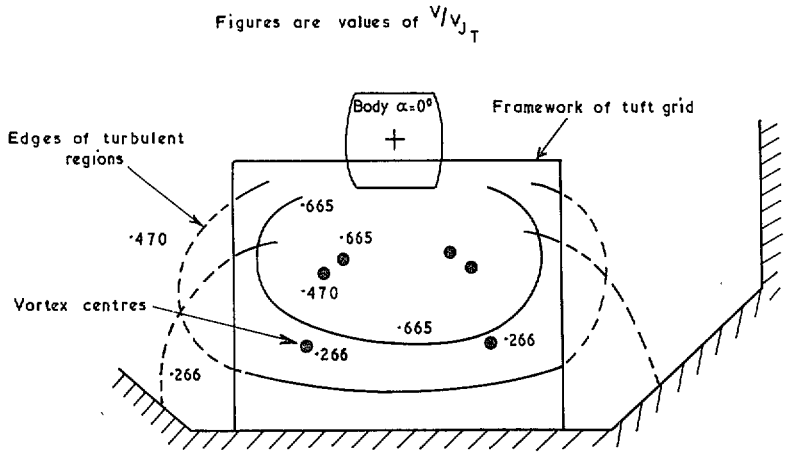

FIG. 10. Jet boundaries and vortex centres 4·2 diameters downstream of jet exit

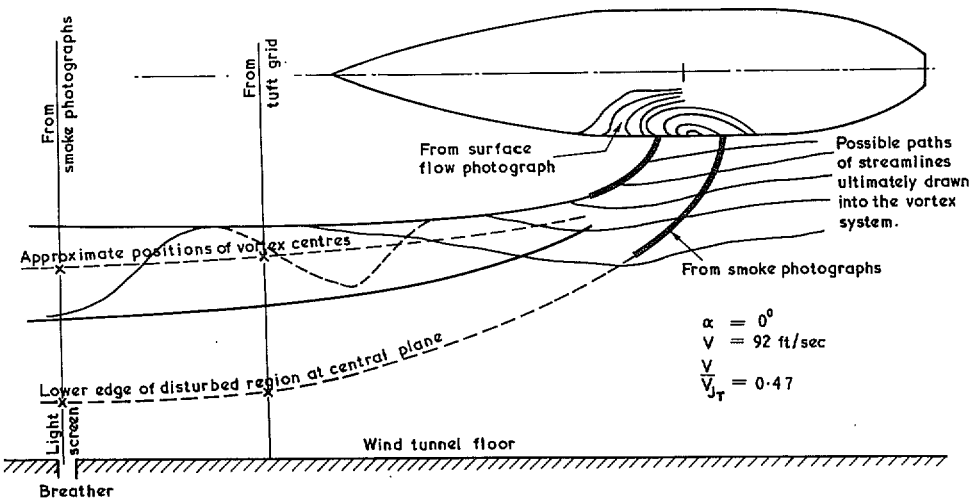

FIG. 11. Possible structure of jet plume, deduced from limited smoke, tuft and surface flow observations

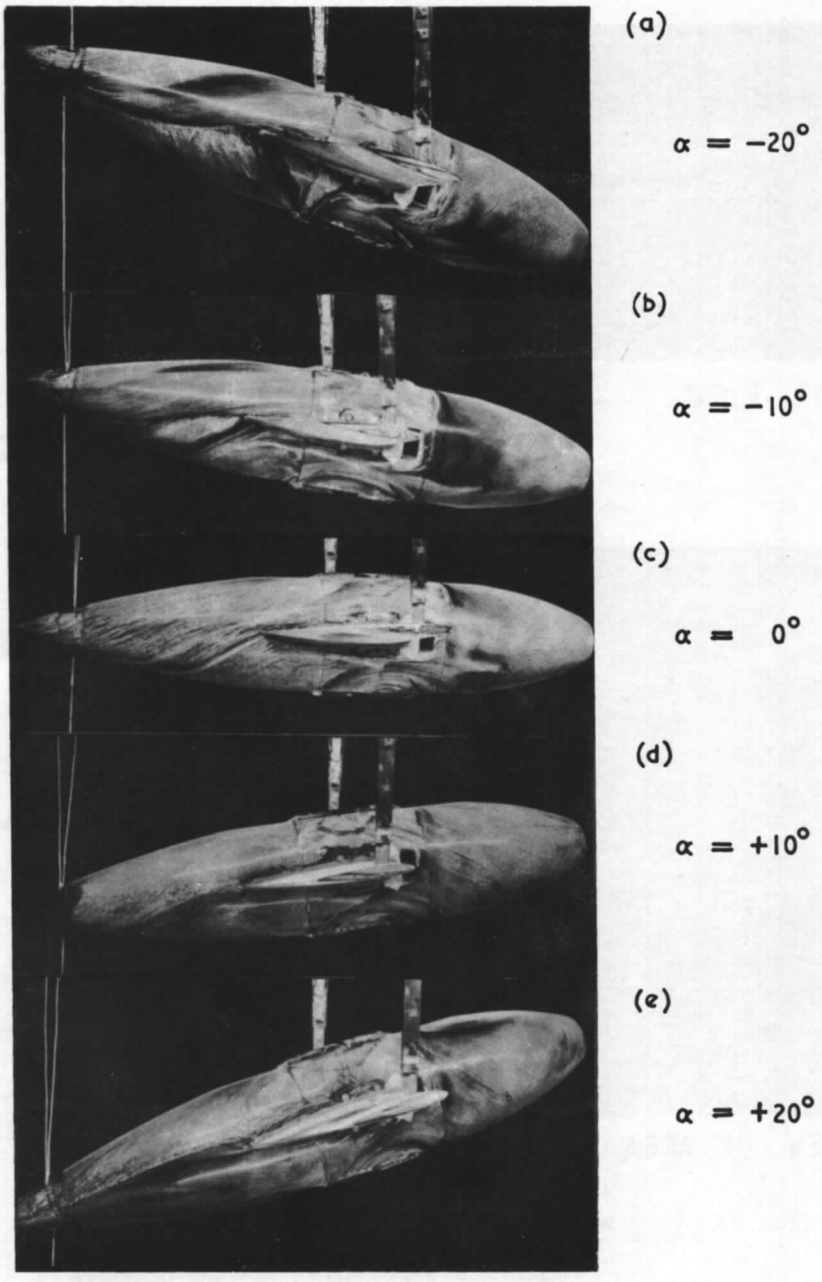

FIG. 12. Body with wings. 136 ft/sec (Fan on). $V/V_{J_T} = 0{\cdot}70$

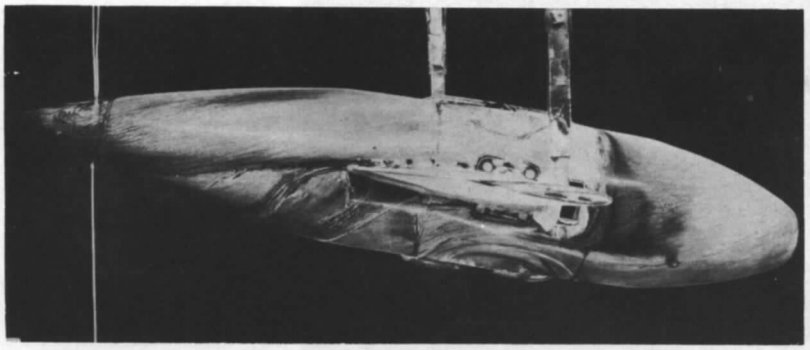

(a)

$\alpha = -10^0$

SIDE VIEW

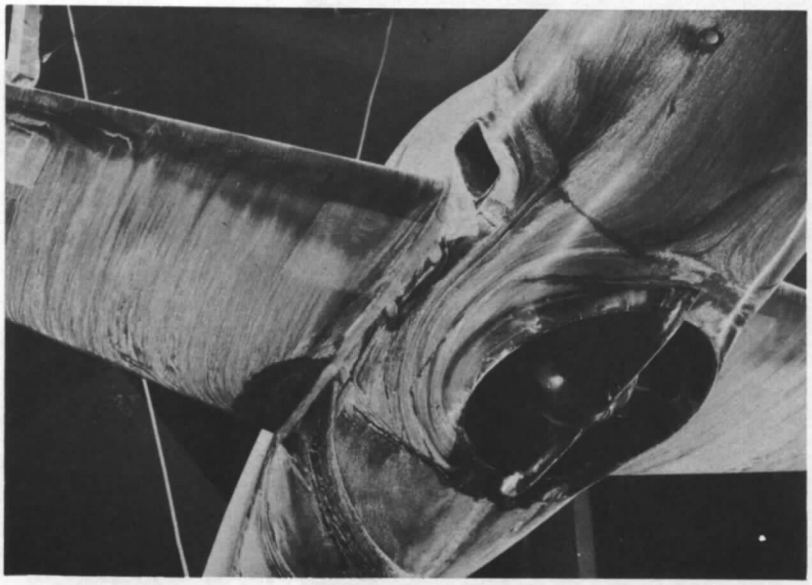

(b)

$\alpha = -10^0$

VIEW OF AREA AROUND JET EXIT

FIG. 13. Body with wings. 93 ft/sec (fan on). $V/V_{J_T} = 0{\cdot}48$

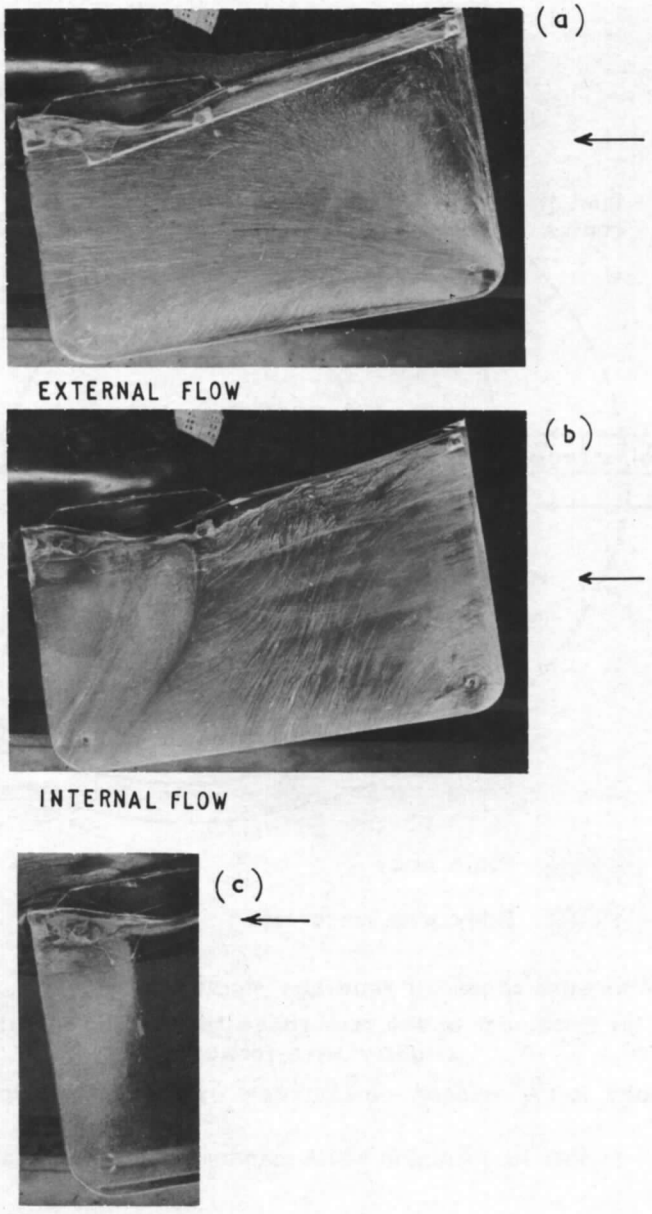

FIG. 14. Flows over perspex underfins (fan on). 93 ft/sec $\alpha = +10°$ $V/V_{J_T} = 0{\cdot}49$

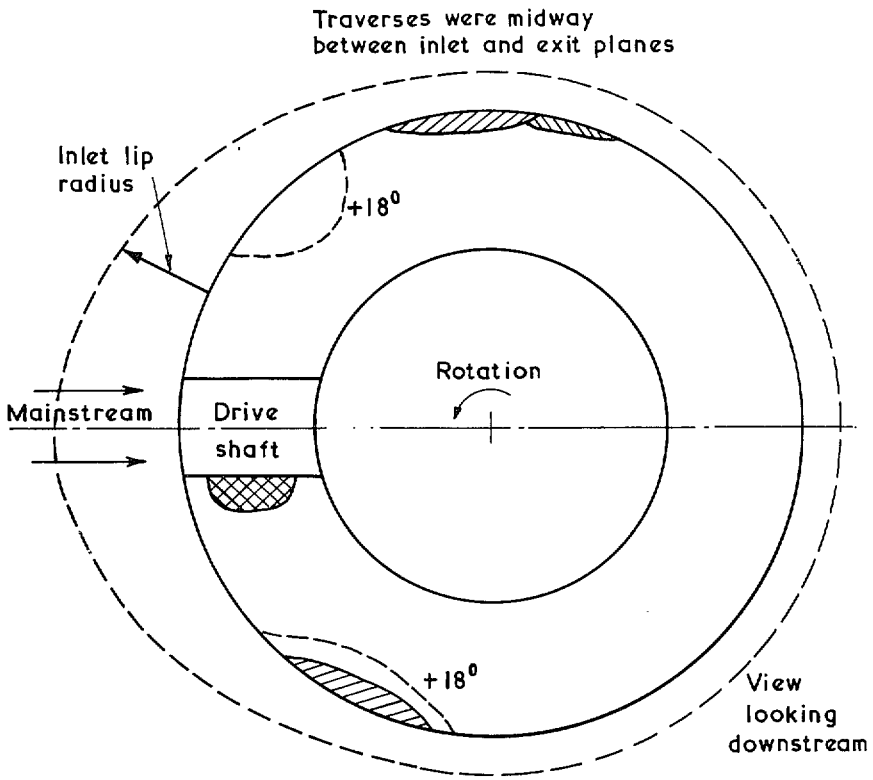

At zero forward speed all readings fluctuated.

Within the remainder of the test range the shaded areas increased only slightly with forward speed

This plane is 1½″ approx downstream of fan and 4″ from the inlet plane

FIG. 15. Areas in which manometer readings fluctuated

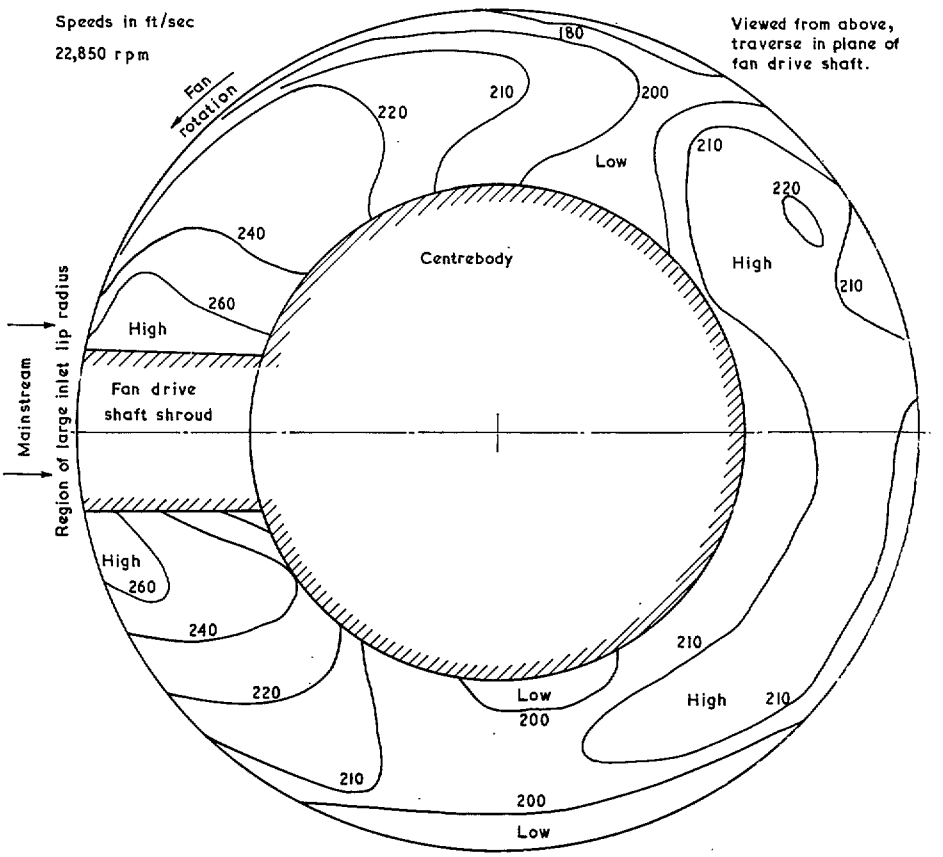

FIG. 16. Distribution of axial velocity between fan and straighteners (Tunnel speed zero)

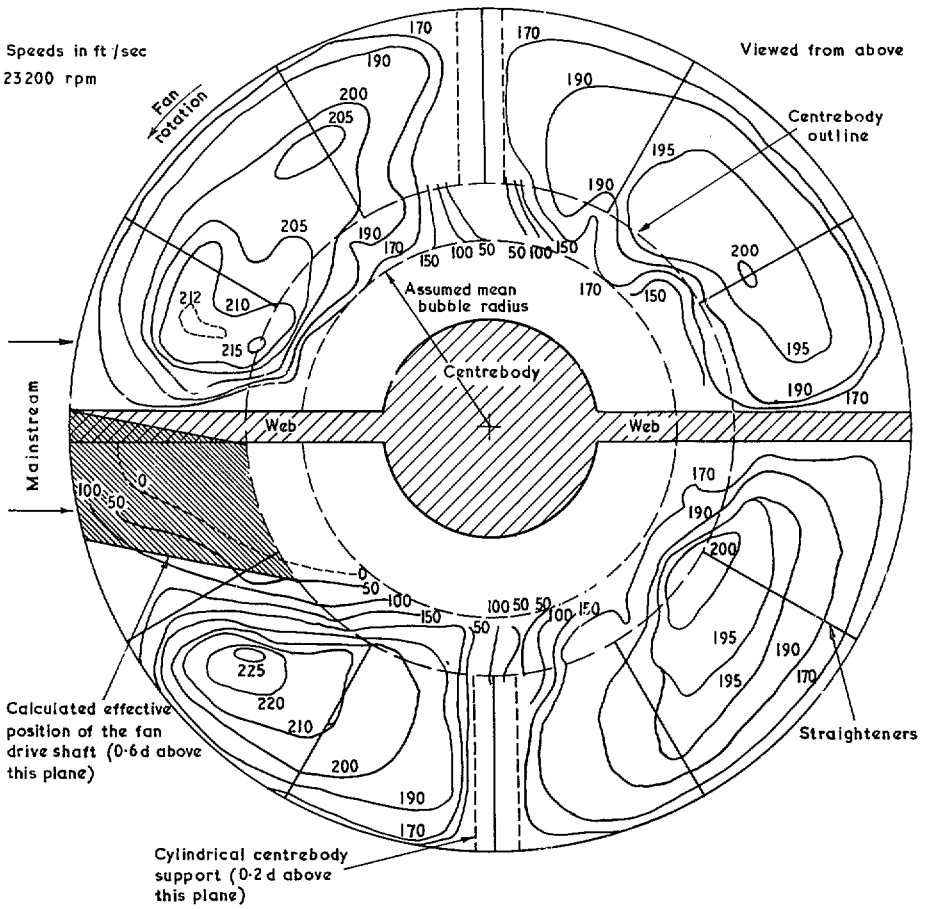

FIG. 17. Axial velocity distribution at the duct exit plane. (Tunnel speed zero)

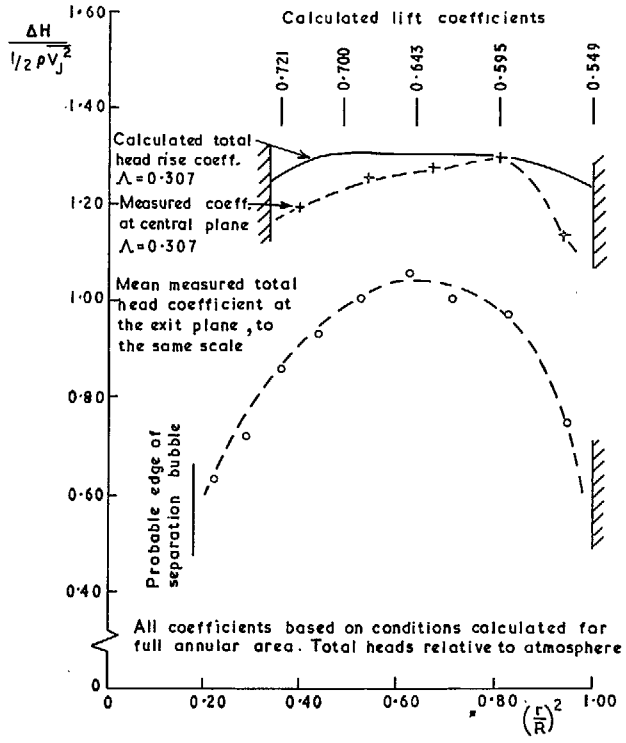

FIG. 18. Radial total-head distributions in static-lift condition

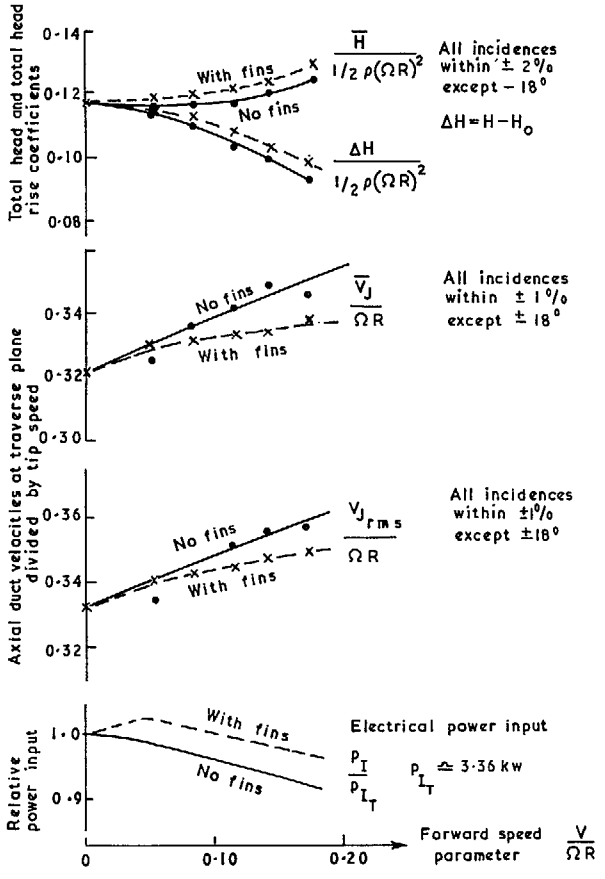

FIG. 19. Plain body, $\alpha = -6$ deg. Variation of mean duct conditions with forward speed

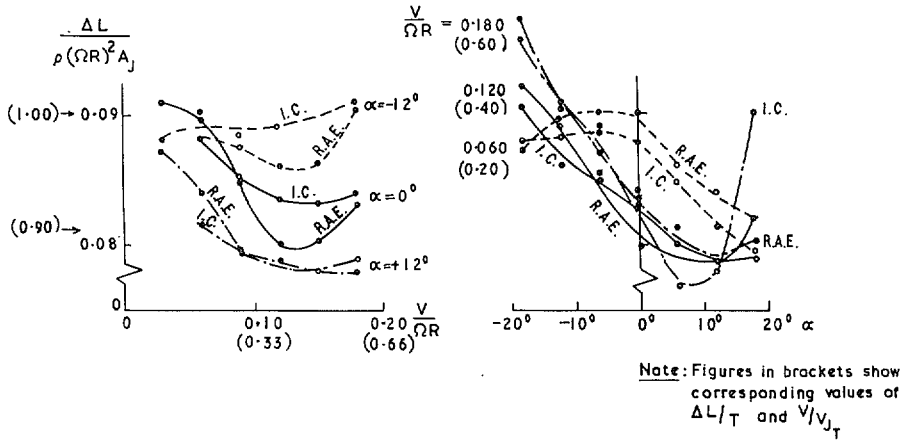

FIG. 20. Plain body. Lift increments in the I.C. 5 ft × 4 ft tunnel and in the R.A.E. No. 1 $11\frac{1}{2}$ ft × $8\frac{1}{2}$ ft tunnel

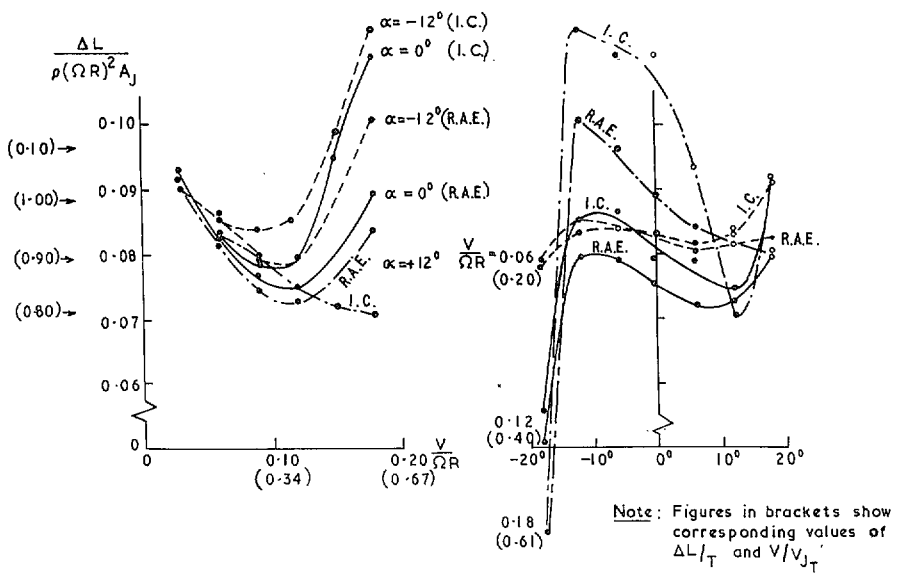

FIG. 21. Body with wings. Lift increments in the I.C. 5 ft × 4 ft tunnel and the R.A.E. No. 1 $11\frac{1}{2}$ ft × $8\frac{1}{2}$ ft tunnel

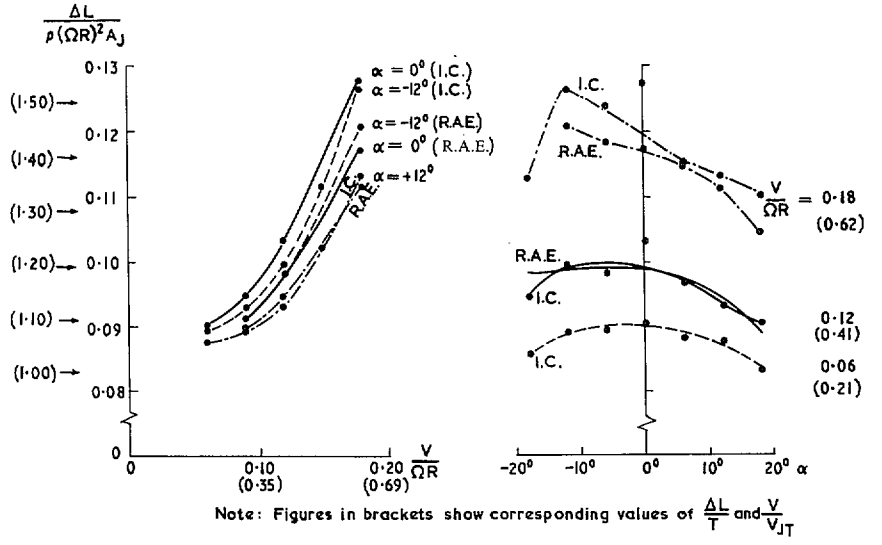

Body without wings but with underfins

FIG. 22. Lift increments in the I.C. 5 ft × 4 ft tunnel and the R.A.E. $11\frac{1}{2}$ ft × $8\frac{1}{2}$ ft No. 1 tunnel

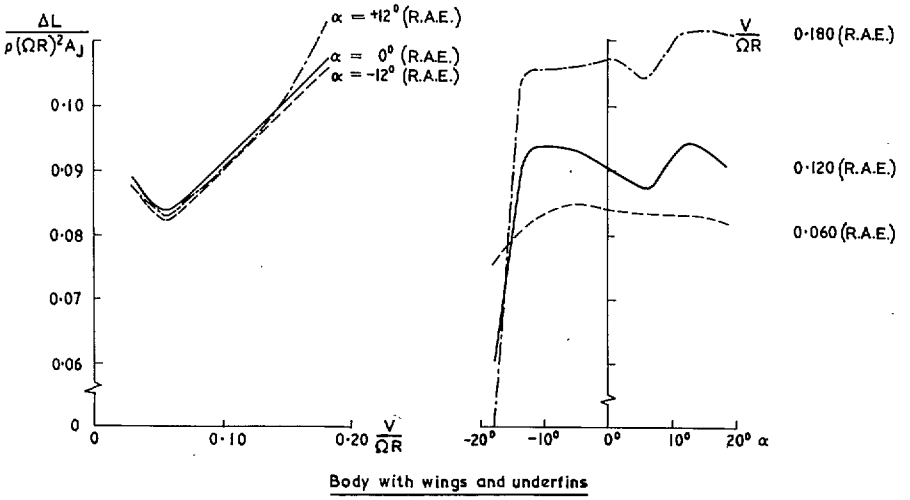

FIG. 23. Lift increments in the R.A.E. No. 1 $11\frac{1}{2}$ ft × $8\frac{1}{2}$ ft tunnel
(No tests performed in the 5 ft × 4 ft tunnel)

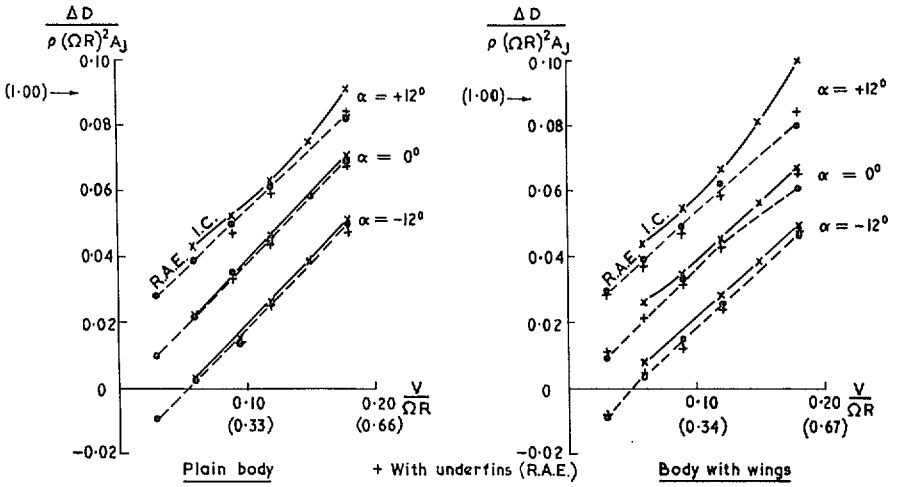

FIG. 24. Drag increments in the I.C. 5 ft × 4 ft tunnel and the R.A.E. No. 1 $11\frac{1}{2}$ ft × $8\frac{1}{2}$ ft tunnel

(Figures in brackets show corresponding values of $\frac{\Delta D}{T}$ and $\frac{V}{V_{J_T}}$)

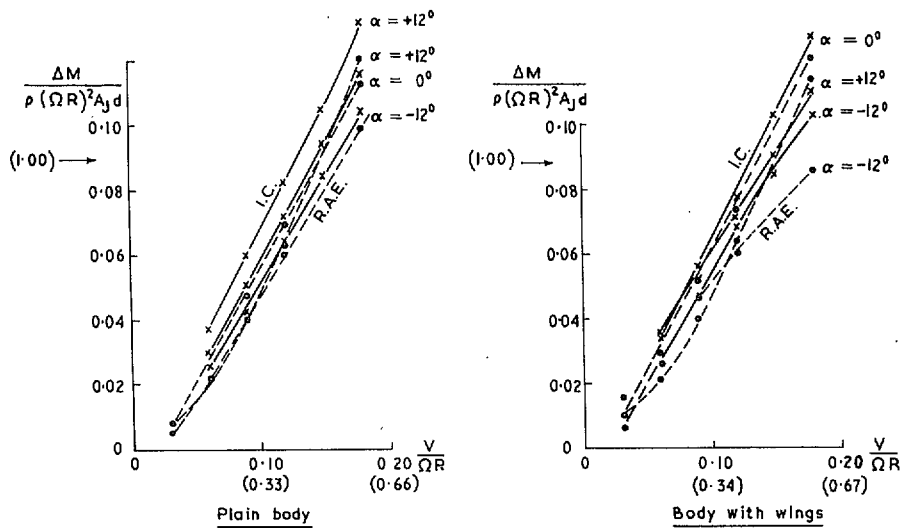

FIG. 25. Pitching moment increments, nose up, in the I.C. 5 ft × 4 ft tunnel and the R.A.E. No. 1 $11\frac{1}{2}$ ft × $8\frac{1}{2}$ ft tunnel

(Figures in brackets show corresponding values of $\frac{\Delta M}{Td}$ and $\frac{V}{V_{J_T}}$)

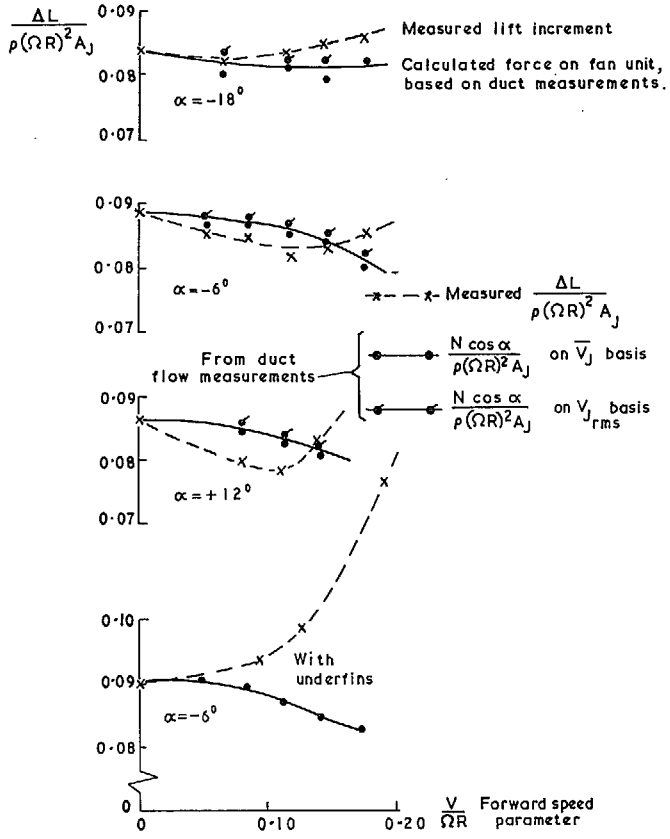

FIG. 26. Plain body. Measured lift increments and estimated forces on the lifting unit

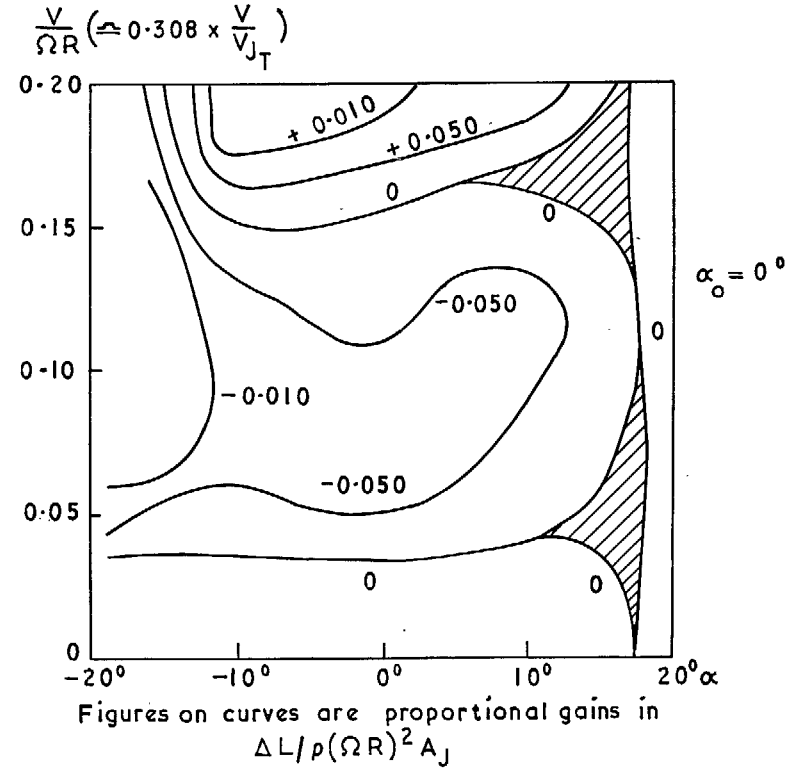

FIG. 27. Incremental lift gains due to the addition of wings to the plain body. $\alpha_0 = 0°$ (5 ft × 4 ft tunnel)

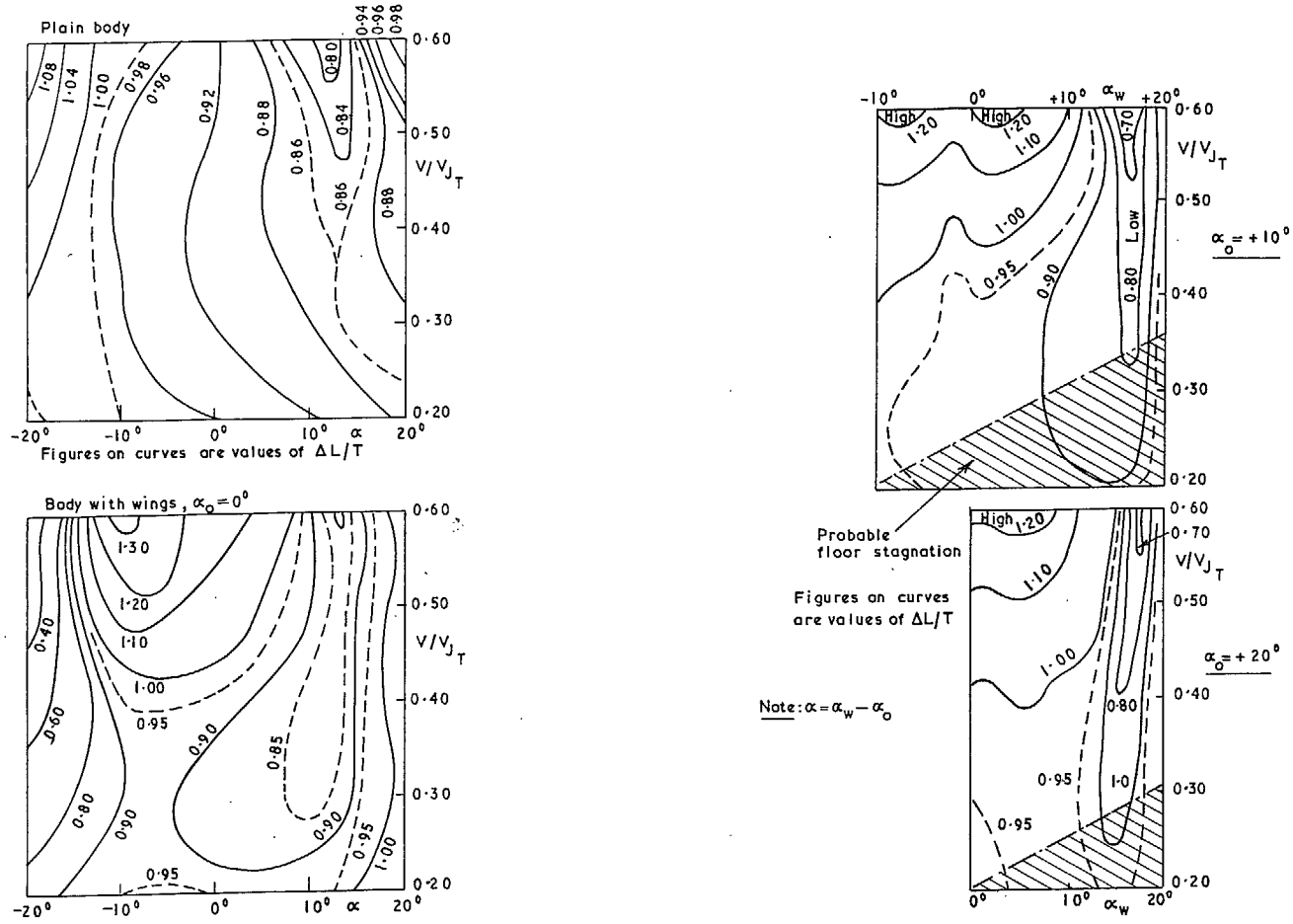

FIG. 28. Variation of lift increment with V/V_{J_T} and incidence. Plain body and body with wings (no fins). Contours of constant lift increment for various wing-setting angles, α_0. (5 ft x 4 ft tunnel).

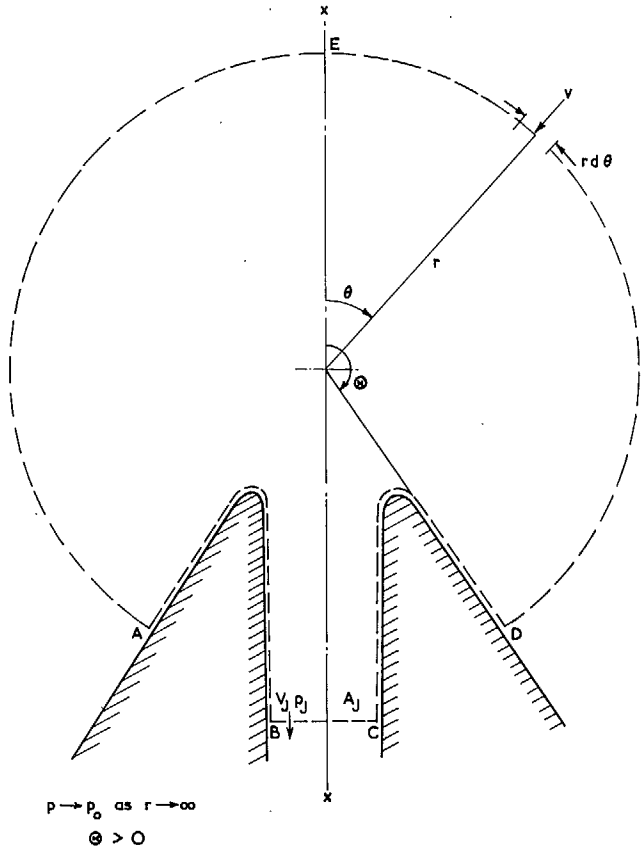

FIG. 29. Control volume for three dimensional inlet without mainstream

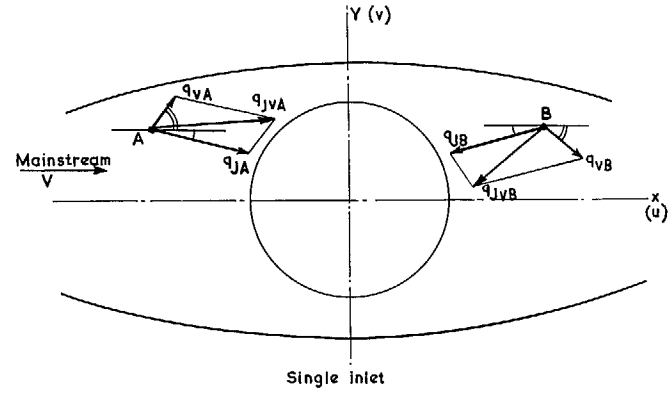

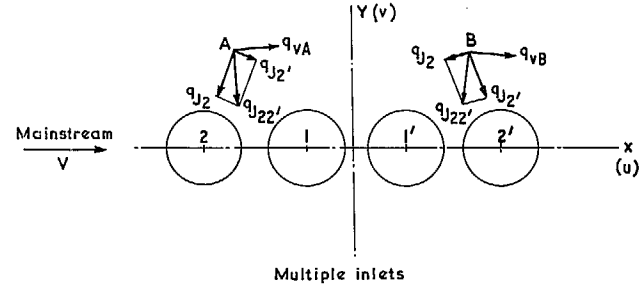

FIGS. 30 and 31. The addition of velocities due to fans and mainstream acting separately

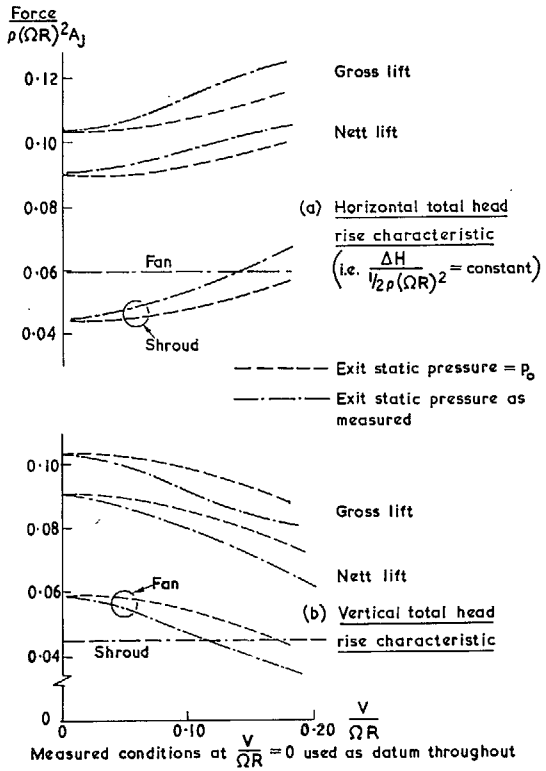

FIG. 32. Breakdown of forces on two idealised lifting units. (Forces acting on the surface around the exit are excluded)

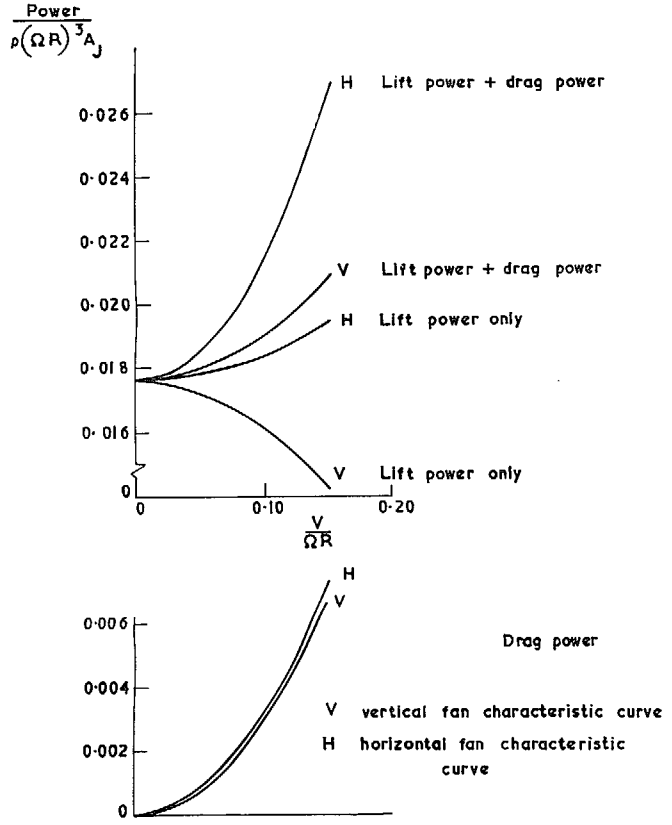

FIG. 33. Power absorbed by two idealised lifting units

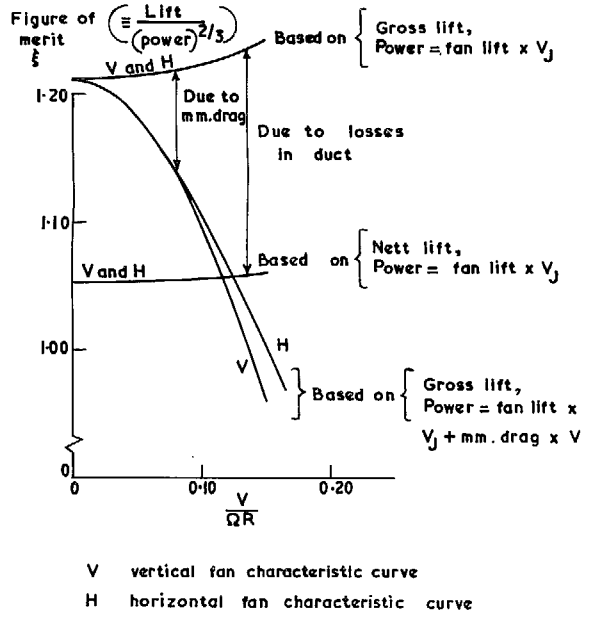

FIG. 34. Figures of merit for two idealised lifting units

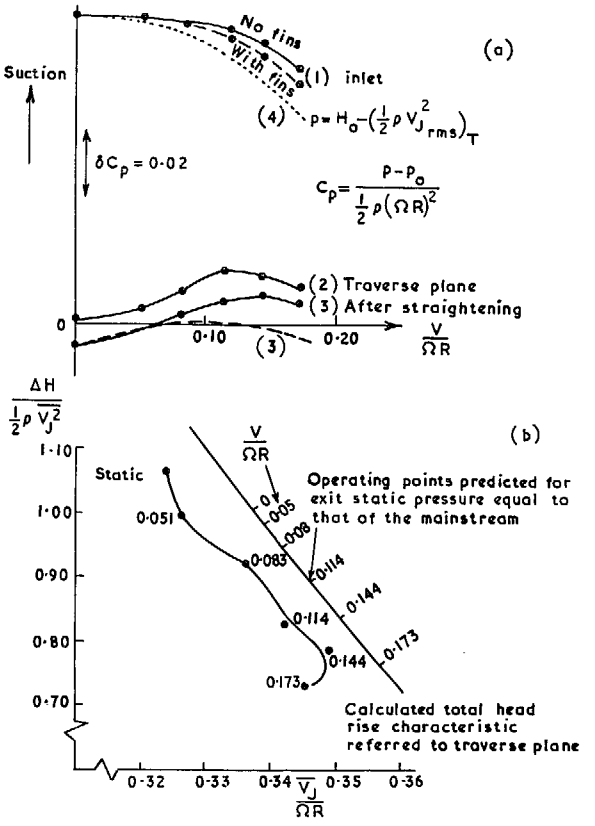

FIG. 35. (a) The variation of duct static pressures with forward speed

(b) Total head rise characteristic at forward speed

Printed in Wales for Her Majesty's Stationery Office by Allens Printers (Wales) Limited.
Dd.125874 K5

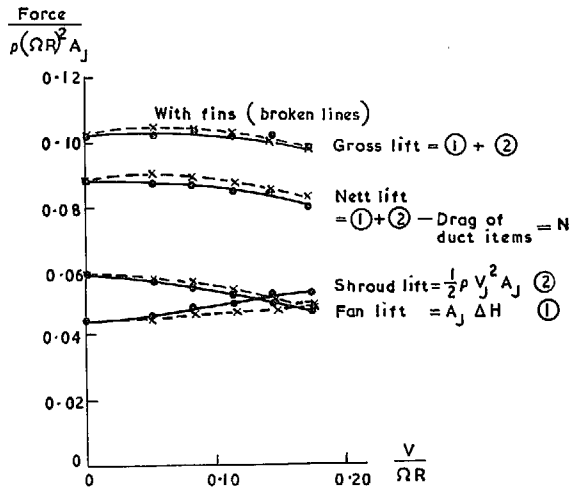

FIG. 36. Breakdown of forces on the lifting unit.

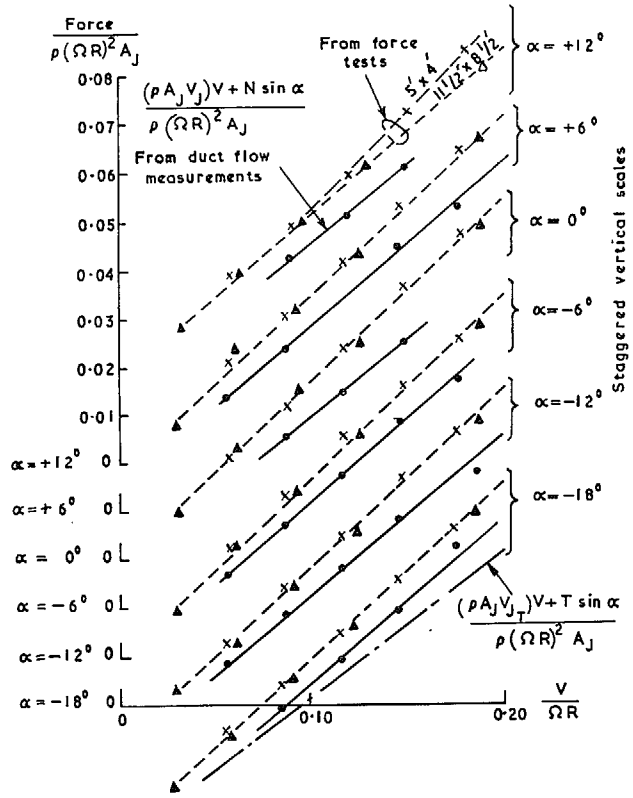

FIG. 37. Isolated body. Measured drag increments and estimates from duct flow measurements

Published by
HER MAJESTY'S STATIONERY OFFICE

To be purchased from
49 High Holborn, London W.C.1
423 Oxford Street, London W.1
13A Castle Street, Edinburgh 2
109 St. Mary Street, Cardiff
Brazennose Street, Manchester 2
50 Fairfax Street, Bristol 1
35 Smallbrook,Ringway, Birmingham 5
7–11 Linenhall Street, Belfast 2
or through any bookseller

S.O. Code No. 23–3470